A COMPARISON OF SATELLITE WINDS AND SURFACE BUOY WINDS

By

Nancy Bepple

B. Sc. (Combined Computer Science/Mathematics) University of Victoria, 1985

A THESIS SUBMITTED IN PARTIAL FULFILLMENT OF

THE REQUIREMENTS FOR THE DEGREE OF

MASTER OF SCIENCE

in

THE FACULTY OF GRADUATE STUDIES

ATMOSPHERIC SCIENCE

We accept this thesis as conforming

to the required standard

THE UNIVERSITY OF BRITISH COLUMBIA

September 1990

In presenting this thesis in partial fulfilment of the requirements for an advanced degree at the University of British Columbia, I agree that the Library shall make it freely available for reference and study. I further agree that permission for extensive copying of this thesis for scholarly purposes may be granted by the head of my department or by his or her representatives. It is understood that copying or publication of this thesis for financial gain shall not be allowed without my written permission.

Department of Geography

The University of British Columbia
Vancouver, Canada

Date Sep 25/90

Abstract

This thesis investigates the relationship between open hexagonal cell cloud motion and surface winds in the northeast Pacific Ocean. Cloud targets are tracked using an automatic scheme fashioned after Barnea and Silverman's (1972) Sequential Similarity Detection Algorithm. The cloud motion vectors obtained are comparable to results obtained by tracking the same cloud targets manually. The well-organized character of open hexagonal cells permits a comparison of various methods of estimating the height of the cloud motion vectors. One method, which uses the minimum infrared pixel value, and a second method, which establishes an arbitrary minimum cloud top temperature, are both found to be unsuitable because of cirrus contamination and partially cloud filled pixels. The cloud motion winds for open hexagonal cells and disorganized cumulus clouds are compared with winds measured at collocated surface buoys. The lack of directional shears between open hexagonal cell movements and surface winds, and directional shears of 14° to 27° for the disorganized cumulus clouds, agree with other observations for the two types of clouds. The differences between the two cloud types suggests that any estimate of surface winds from cloud motion should include cloud type information.

Table of Contents

List of Tables

List of Figures

Acknowledgement

Larry Diehl, my one time supervisor and long time mentor, influenced me greatly when I decided to return to school and study atmospheric science. He gave me my initial training in the meteorology and encouraged me to pursue further studies. Once at UBC, Phil Austin was the steering force to my studies and the eventual completion of this thesis. His patience and enthusiasm kept me going in the right direction. I would like to thank both of them for the difficult and often thankless task of giving me guidance.

MacDonald Dettwiler and Associates, and the B.C. Science Council provided me with funding which gave me the opportunity to return to school. I look forward to returning to M.D.A. and applying my new skills.

The research could not have been done with the assistance of John Spagnol and Reg Dunkley, and other personnel of the Pacific Weather Centre, who gave me access to their computer facilities, weather observations and expertise.

And thanks to Judy, Ken, Jane, Pamela and Pat for being there.

Chapter 1

Introduction

Since the 1960's, atmospheric winds (speed and direction) have been estimated using cloud motions measured from sequential satellite images. The vectors representing such cloud movements account for a large portion of all low (0 to 2km), medium (2 to 7km) and high (7 to 10km) level wind information collected by meteorological agencies, especially over oceans, where surface wind reports, and upper air radiosonde data are sparse. To calculate the cloud motion wind, a cloud parcel is selected on the first of two temporally sequential geostationary satellite images. On the second image, the new location of the cloud parcel is found. The speed and direction of the cloud parcel is calculated from the displacement of the cloud parcel and the time period between the two images. This vector is called the cloud motion wind.

At the Pacific Weather Centre (PWC), in Vancouver, B.C., cloud motion winds are collected hourly and are used by operational meteorologists to update marine forecasts off the west coast of Vancouver Island. These wind estimates are often the first indication of the development of storm force or gale force winds that can threaten fisherpersons' safety. Collection of cloud motion winds at the PWC is currently performed manually: the forecaster chooses a cloud target on a first image and finds its new location on a second image. Once a target has been tracked, its height is estimated using the temperature of the cloud, determined from infrared satellite imagery and a representative vertical temperature profile as provided by a radiosonde observation at a nearby shore station or by TOVS, the polar-orbiting TIROS-N satellite's radiometric vertical sounder. The cloud

motion wind is then used to estimate the surface wind. The clouds that are tracked are low level clouds, with their tops below 3km. The PWC does not have a standard method of interpolating the motion of the cloud field down to the surface. Some forecasters use the cloud motion wind directly as an estimate of the surface wind. Other forecasters reduce the wind speed and change the wind direction based on a simple Ekman boundary layer model (personal communications with PWC personnel, 1989 and 1990). Chapter 4 contains a further explanation of this model.

While the PWC uses cloud motion winds extensively for surface marine forecasts, their present approach has a number of shortcomings. First, manually tracking cloud motions is labourious and time consuming. A trained forecaster at the PWC only has time to track about 6 to 8 cloud targets per hour. Second, assigning the height of the cloud motion wind is inaccurate because of partially filled cloud pixels, and overlaying cirrus contamination. Third, because of the height uncertainty of the cloud motion wind, and because the relationship between winds aloft and surface winds is complex, estimating the surface wind field from measured cloud motions is difficult. These problems are by no means unique to the PWC. In the last 30 years, the two main areas of research in measuring winds from cloud motions have been in implementing methods for tracking clouds automatically, and in estimating the appropriate height. In recent years, in order to expand the usefulness of the cloud motion wind data, researchers have attempted to use it to estimate surface wind data.

Despite the operational use of cloud motion winds at the PWC as input into surface marine forecasts, no studies have yet been undertaken to investigate the relationship between cloud motion winds and observed surface winds in the northeastern Pacific Ocean. This current research will supplement the forecasters' experience by examining this relationship for a specific type of cloud which occurs frequently in this region during the winter months: open hexagonal cells. In order to meet this objective, the problems

of tracking the clouds and assigning the vectors to a specific atmospheric level will also be addressed.

There are three parts to the investigation. First, rather than using a manual method for tracking the clouds, as is done at the PWC, a semiautomatic scheme developed by Barnes and Silverman (1972) was used. The semiautomatic scheme was chosen both to aid in the collection of cloud motion winds and to evaluate its effectiveness at higher latitudes. At higher latitudes, there is less spatial resolution in geostationary satellite images and more distortion of the cloud elements because of the increased viewing angle of the satellite. The other two facets of the study deal specifically with open hexagonal cells. For both of these parts, the structure of the open hexagonal cells was used to investigate the problems. Methods for estimating the height of open hexagonal cell cloud motion winds were examined. The cloud motion winds were compared to surface buoy reports.

1.0.1 Previous Work

Previous works on the relationship between cloud motion winds and surface winds has concentrated on tropical regions. Studies by Wylie and Hinton (1981, 1982), Sadler and Kilonsky (1985), Hamada (1985), and Halpern and Knox (1983) have investigated the relationship between low level cloud motions and surface wind reports in the tropics. Wylie and Hinton compared low level cloud motion winds with ship observations of surface winds in the Indian Ocean. The ocean region was divided into 6 regions, ranging in size from (3000km x 1000km) to (7000km x 1500km). The cloud motion winds for each region were objectively analyzed onto a uniform grid, and then compared with ship reports within the same region. Results indicated that surface winds could be estimated by subtracting the mean wind shear between the cloud level and the surface of the region from cloud motion winds. While this approach may be used to estimate the large scale

surface flow, it cannot be relied on to predict the winds at a specific location. A region as large as (3000km x 1000km) can contain 2 or 3 synoptic scale systems, within which large variations in the vertical wind shear will be observed.

Sadler and Kilonsky, and Hamada were both able to estimate monthly mean surface winds in the Pacific Ocean. Sadler and Kilonsky derived monthly mean surface winds for the tropical Pacific Ocean from cloud motion vectors by using climatological values of the vertical shear between ship winds and cloud motion winds. Hamada used multiple-linear regression to derive monthly mean surface winds for the western Pacific. While this monthly wind data is useful in modeling of the long term wind-driven ocean circulation, it cannot be applied to short range (6-12 hours) or midrange (12-48 hours) synoptic scale weather forecasting.

In Halpern and Knox's study, cloud motion winds within a 5° latitude by 5° longitude box, located in the Pacific Ocean at the equator, were compared with data from a buoy positioned in the center of the region. Over an 11 month period, the two data sets were found to be essentially uncorrelated on a daily basis. However, there was a correlation when the data was averaged over a 15-day period. A shortcoming of Halpern and Knox's study is that they do not distinguish between the different types of clouds that were tracked during their study. Results from numerical boundary layer models constructed by Brown and Liu (1982) found that depending on the convective stability of the air, surface wind speeds can be 0 to 80% weaker than winds at the level of low-level clouds, while directional differences can vary from 10° to 24°. Their model results were verified by surface buoy measurement and upper-level winds measured by the SEASAT-A polar-orbiting satellite's scatterometer (Brown and Levy, 1986). Different stability regimes not only result in a variation in the relationship between winds aloft and surface winds, but also generate different types of clouds.

Rather than study the relationship between the large scale surface wind field and cloud

motion winds, this study will compare the two wind measures at a specific location. Only open hexagonal cells, a type of organized convective cloud, will be tracked.

1.0.2 Organized Convective Cells

Open hexagonal cells, along with cloud streets and closed hexagonal cells, are three types of cumulus clouds that have a high degree of horizontal and vertical organization. Figure 2.3 is a beautiful example of open cells and cloud streets. It is not coincidental that the two cloud types are in the same region. They, along with closed cells, are generated by meteorological conditions that are necessary for organized, rather than disorganized convection to occur. For organized convection to occur, there must be a stable, low-level capping inversion, moderate surface heat flux and low wind shears between the surface and the tops of the clouds.

Bénard was the first to report observations of organized convection, with a predominantly hexagonal pattern, now called Rayleigh-Bénard cells, in a pan of oil. Rayleigh, using the linearized two-dimensional Navier-Stokes equations of motion with rigid, stress-free conducting boundaries, showed that infinitesimal perturbations will grow only when a non-dimensional parameter,

$$Ra \equiv \frac{g\Gamma h^4}{T_m \nu \kappa} \tag{1.1}$$

now called the Rayleigh number, Ra, exceeds a critical value. Here h is the depth of the layer; $-\Gamma$ is the temperature gradient of the layer; T_m is the mean temperature of the fluid; ν is the fluid's kinematic viscosity; κ is its thermal diffusivity; g is the acceleration of gravity. The parameters in 1.1 govern the ability of a fluid, heated from beneath and cooled from above, to overturn. A large negative temperature gradient (warm, light air below cold, heavy air), or small values of kinematic viscosity or thermal diffusivity, make it easy for buoyant convective parcels to rise to the upper boundary, without diffusing

away the buoyancy difference between parcel and surrounding fluid which is driving the ascent.

The type of convection - turbulent (disorganized clouds) , three dimensional (open or closed cells), two dimensional (cloud streets), or no convection - is determined by the relationship between the Rayleigh number, Ra, and the Prandtl number, Pr,

$$Pr \equiv \frac{\nu}{\kappa} \tag{1.2}$$

Krishnamurti (1970,1975a) conducted a series of experiments into shallow horizontal convection using a tank with heating on the bottom plate and cooling on the top. Her results (figure 1.1) show how for a specific fluid, characterized by Pr, there are a number of transitions between no motion and turbulence. Below the critical Rayleigh number, there is no convection, and all of the heat from the lower plate is moved through the layer by conduction. As the Rayleigh number increases, convection with a 2-dimensional roll structure occurs. There is then a transition to 3-dimensional cell structures. At sufficiently large Rayleigh numbers the flow becomes turbulent.

In the atmosphere, molecular dissipation must be replaced by turbulent diffusion, and water phase change complicates the picture. To calculate Ra in the presence of small scale turbulence, an analogy is often made between the mixing effects of turbulent eddies and molecular conduction and dissipation. Krishnamurti (1975b) used an eddy viscosity, $\nu_e = 3x10^5 cm^2 s^{-1}$ in place of the atmospheric kinematic viscosity of $1.4x10^{-5} cm^2 s^{-1}$, and eddy diffusivity, $\kappa_e = 1x10^5 cm^2 s^{-1}$ in place of the atmospheric thermal diffusivity of $2x10^{-5} cm^2 s^{-1}$. Therefore, her Prandtl number lies around 3.0, which means we might expect rolls for $2 * 10^3 < Ra < 10^4$ and cells for $10^4 < Ra < 5x10^5$, if Krishamurti's findings are applicable to the atmosphere. Krishnamurti (1975b) calculated Ra for two cases of open hexagonal cells, using nearby rawindsonde observations, and found values from $3x10^4$ to $5x10^4$.

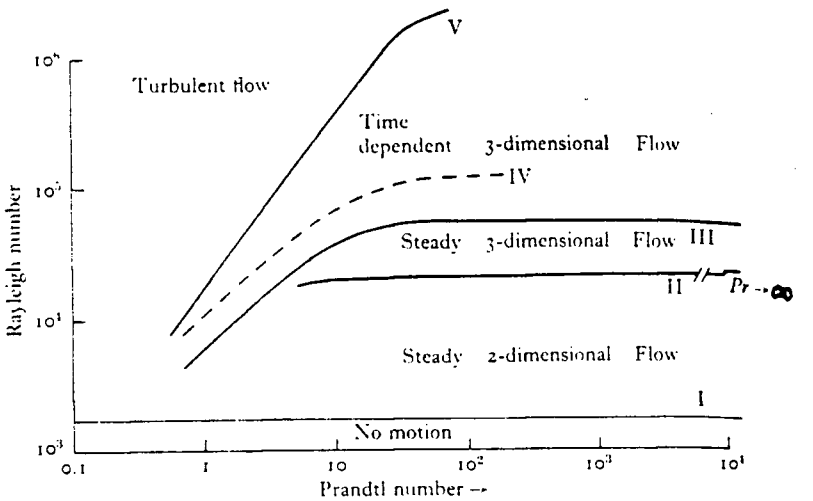

Figure 1.1: Convective regimes for various values of Ra and Pr (from Krishnamurti, 1970). The Prandtl number for air is approximately 0.7.

For the three organized convective clouds, the basic building block of the circulation is a box. For open cells, air rises along one of the vertical sides of the box as buoyancy is introduced at the bottom. Across the top of the box, this buoyancy is dissipated through thermal dissipation. When all of the buoyancy is dissipated, the air descends on the other vertical side of the box. The air then moves along the bottom of the box picking up buoyancy, until it reaches the start of the cycle again. The limits on Ra noted above limit the height of a layer that can produce organized convection. There are also limits on the width of the box. Small box widths are discouraged because the rapid horizontal variations between updrafts and downdrafts will generate turbulent mixing and destroy the organized circulation. Since the air cannot descend until all of the buoyancy has been dissipated, the rate of thermal dissipation, which is determined by κ, limits the maximum width of the box. The circulation of closed cells is much the same but in reverse, with the

convection being driven by radiative cooling at the cloud tops which creates a downward buoyancy force. Further explanations of organized convection can be found in Turner (1973) and Van Delden (1987).

For organized clouds to form there is typically an inversion at about 3km or lower. The inversion acts as the upper plate, capping the convection at a shallow level, and inducing a linked downward flow. Cloud streets form as tubes parallel to the mean wind of the layer. The air ascends on one side of the tube until it reaches the inversion, and descends on the other. Adjacent tubes are linked, with air either ascending or descending between each pair. By ascending into the shear the perturbations are able to extract energy from the mean flow. For open cells, air rises in the rings forming clouds, and descends in the centers of the rings, where it is clear. The opposite is true for closed cells, which are circular areas of clouds, created by rising air, surrounded by clear rings, where the air is descending. The circulation of adjacent open or closed cells is linked, forming a honeycomb-like pattern over the region akin to Rayleigh-Bénard cells. The tops of organized clouds are rarely above 3km: as the depth of the convective layer increases, Ra increases, and convection becomes disorganized. The presence of organized cells also indicates that the vertical extent of the cloud, capped at the level of the inversion, will be roughly uniform throughout the region. If not, the linked circulation of the cells would be destroyed by large discontinuities between the cloud tops of adjacent cells.

As indicated above, organization produces loose coupling between vertical and horizontal length scales of the clouds. In a study, Weston (1980) examined 21 cases of cloud streets and found the aspect ratio of the streets (the ratio of the distance between streets and the height of the layer) to be approximately 3. Agee and Dowell (1974) examined 15 cases of open cells and 28 cases of closed cells. They found that for the open cells, the aspect ratio of the diameter of the cell to the height of the layer was from 6 to 38, while that for the closed cells the aspect ratio was from 14 to 45.

Cellular cloud patterns are also strongly influenced by vertical wind shear. Weak shears are necessary for open and closed cells to form. Agee and Dowell (1974) found shears of the magnitude of $2.3 ms^{-1}km^{-1}$ for open cells and $1.25 ms^{-1}km^{-1}$ for closed cells. They also found weak directional shears for open ($-5.73°$) and closed cells ($6.67°$). Strong shears create a directionality to the convection. Cloud streets can occur in shears of $5.0 ms^{-1}km^{-1}$ (Van Delden, 1987). But larger shears introduce new instabilities and overwhelm the uniform convective mode.

1.0.3 Goals of this Work

This work explores the relationship between surface wind reports and cloud motion winds of a specific cloud type; that of open hexagonal cells. Unlike previous investigations, the study area is in the midlatitudes rather than in the tropics. Measurements for this research were taken in the northeastern Pacific Ocean, where organized cellular convective clouds often occur behind an advancing cold front, or as a result of a cold Arctic outflow into the Gulf of Alaska. While the previous studies used data sets that were large either spatially or temporally, this study is limited in both space and time. Further, whereas the other studies do not distinguish between the different types of low level clouds tracked, this study compares only cloud motion winds for open hexagonal cells with surface winds.

The restrictive requirements for the occurrence of open cells may provide some insight into two difficult problems encountered when estimating surface winds from low-level cloud motions: accurate height assignment and modeling the relationship between winds at the surface and aloft.

Estimating the height of the cloud motion wind is the largest source of error for cloud motion winds (Whitney, 1983). Without an accurate estimate of the height of the cloud motion wind, the task of estimating the surface wind from measurements of cloud movements is more difficult. One aspect of this study is to explore various methods for

estimating the height of the open hexagonal cells.

Another of the difficulties in estimating surface winds is that interactions within the boundary layer are very complex. The pressure gradient force, the Coriolis force, thermal wind shear, surface friction and stability all contribute to the speed and direction of the wind in the boundary layer. Because of the complex relationship between the low-level winds and surface winds, Halpern and Knox found that the surface wind was not correlated with low-level cloud motions on a daily time scale, but was correlated for a 15 day mean. The complexity of the boundary layer is simplified by considering only the cloud motion vectors of open hexagonal cells.

1.0.4 Overview of the Thesis

The three areas of investigation of research are presented in chapters 2 through 4. Chapter 2 describes how the cloud motion data, along with other wind data, are collected. Chapter 3 explores ways to calculate the height of open hexagonal cell cloud motion vectors. The relationship between the cloud motion vectors and the buoy reports are obtained through a number of analysis techniques. These results are detailed in chapter 4. Conclusions drawn from this research are presented in the closing chapter, chapter 5.

Chapter 2

Data Sets

2.1 Cloud Motion Wind Data

There are three steps in estimating wind fields from satellite images.

- Acquiring the satellite images.
- Tracking the cloud targets.
- Estimating the wind speed, direction, and height.

In the following three subsections, each step is outlined. Errors induced by assumptions, instruments, and the tracking algorithms are estimated in the fourth subsection.

2.1.1 Satellite Images

Visible (0.6μm) and infrared (12μm) imagery was collected from the Geostationary Operational Environmental Satellite (GOES) at the Pacific Weather Centre (PWC) using MacDonald Dettwiler and Associates' Meteorological Data Analysis System (METDAS). The PWC system, which is normally used operationally, was made available for data collection on 9 days. Three of the days contained trackable low-level clouds. On 24 November 1989, shown in figure 2.1, open cells ranging from 20 to 115km in diameter were present off the west coast of Vancouver Island. In the center of the image, the less structured areas of cloud are overlaying cirrus. On 5 January 1990 (figure 2.2) disorganized cumulus clouds formed behind an advancing cold front, which is the line of solid

cloud in the bottom right corner. Patches of cirrus reside throughout the image, which may have sheared off the advancing front. Figure 2.3 shows the 16 February 1990 image. Cloud streets, spaced at 7km, were formed by cold air streaming offshore from Alaska and northern B.C. over the warmer water. As the flow moved south, the streets transformed into open hexagonal cells with diameters from 20 to 96km. What little cirrus there is in the scene, appears to be generated in the region of convergence in the right center area of the image, where the cloud streets broke into cells. The other 6 days (19 September 1989, 1 December 1989, 11 December 1989, 15 December 1989, 15 June 1990, 22 June 1990) consisted of untrackable stratus clouds or middle and high clouds.

2.1.2 Cloud Tracking

Clouds were tracked for a pair of visible satellite images separated by a 1/2 hour interval. Individual cloud parcels are tracked by selecting a cloud target on a first satellite image, and then finding its new location on a second satellite image. There are a number of ways that targets can be located.

In some systems, such as those described by Hubert (1979), a user manually selects the original targets, and locates the new positions. This type of approach is currently in use at the PWC. In systems such as McIDAS (Man-Computer Interactive Data Access System) developed at the University of Wisconsin, targets are selected by the operator, and their new locations are calculated using a cross-correlation matching algorithm (Endlich and Wolf, 1981). Other systems are almost completely automated. As an example, in the NASA Marshall Space Flight Center system (Wilson, 1984) cloud targets are selected and tracked objectively, with no operator input. Wilson compared cloud motion winds from this system with those generated by a manual system and found both systems generated comparable flow fields and were statistically similar. While experimental results have found errors as low as $2ms^{-1}$ for cloud motion wind estimates, when Bengtsson et al

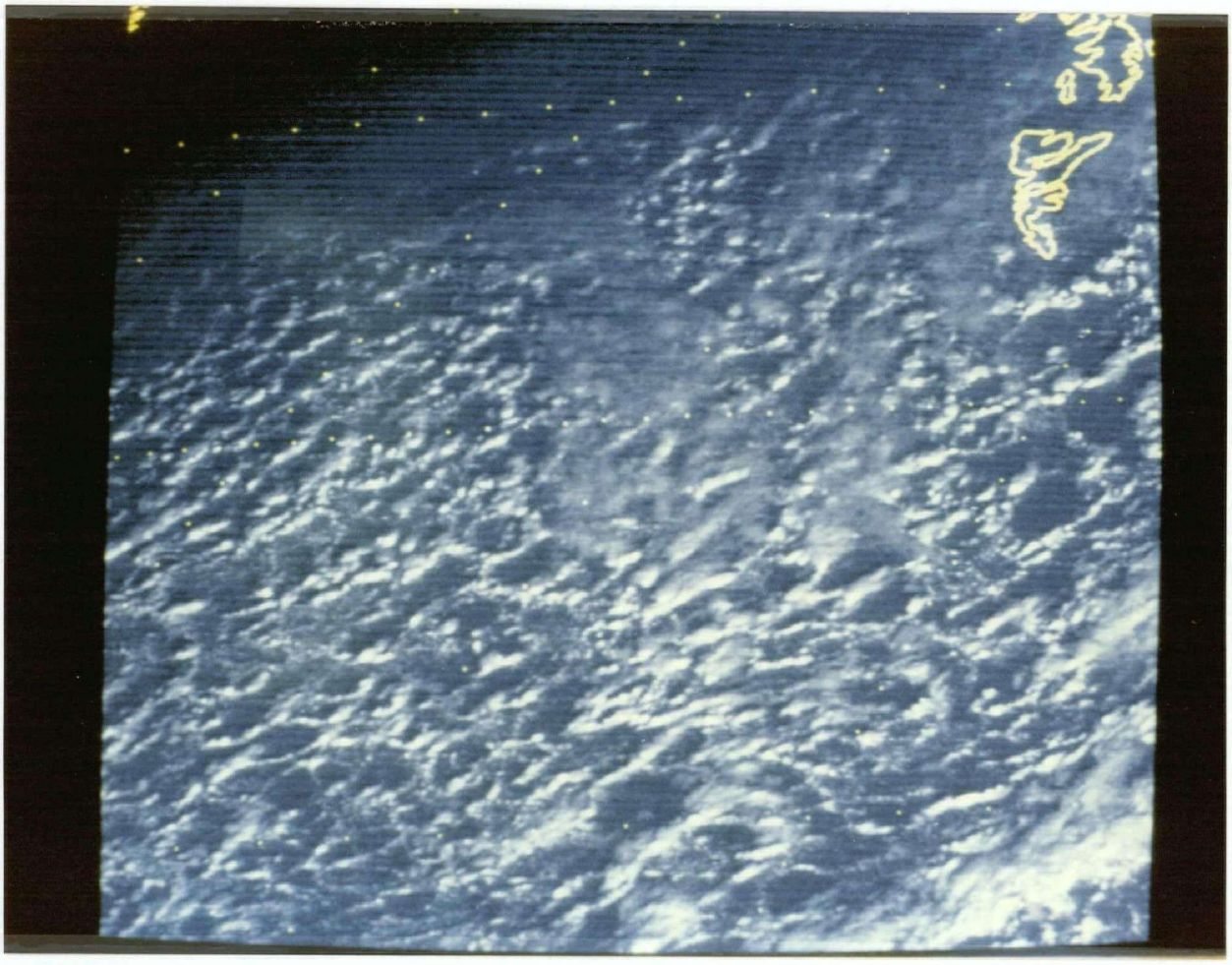

Figure 2.1: 24 November 1989, 17:30Z, visible channel

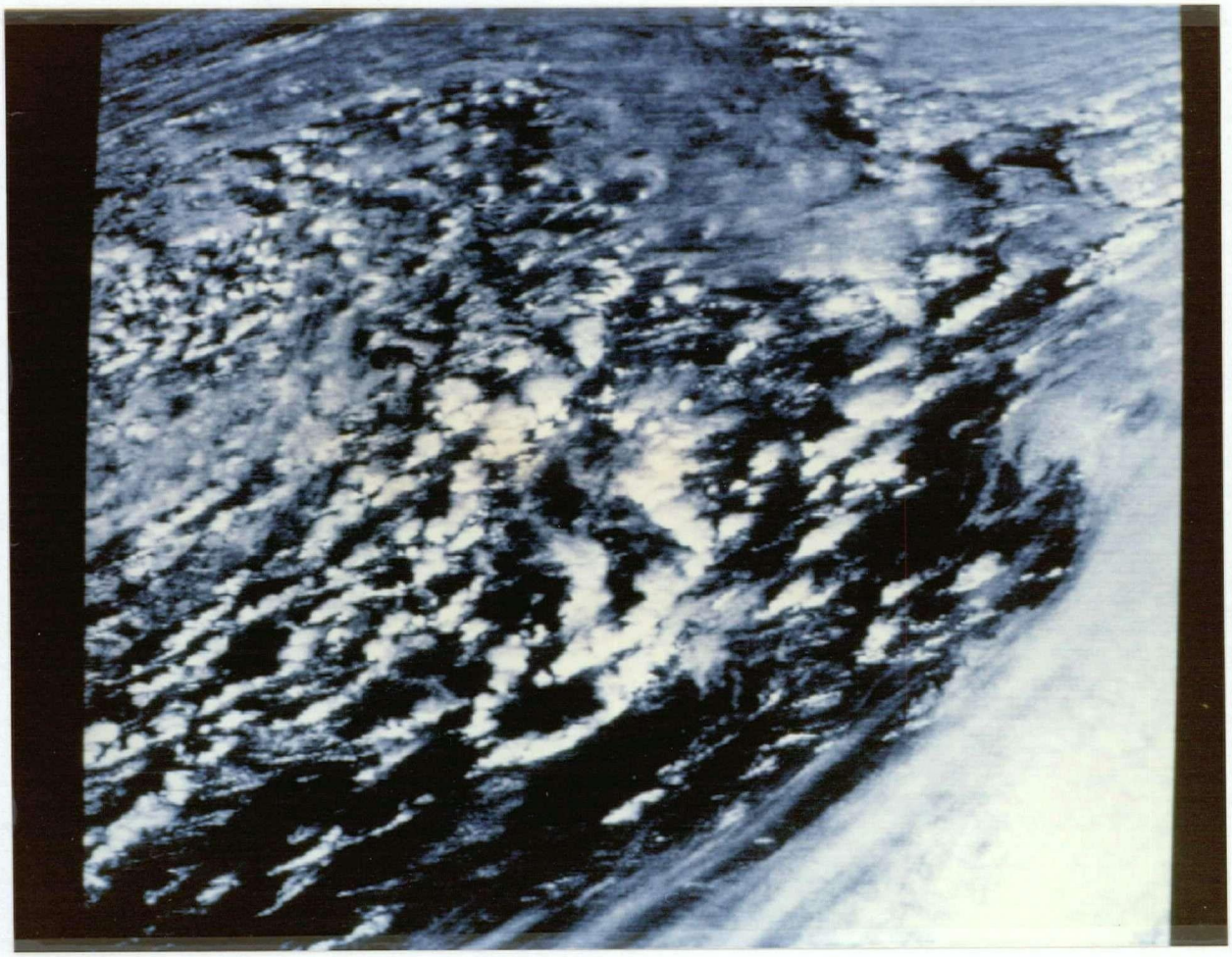

Figure 2.2: 5 January 1989, 20:00Z, visible channel

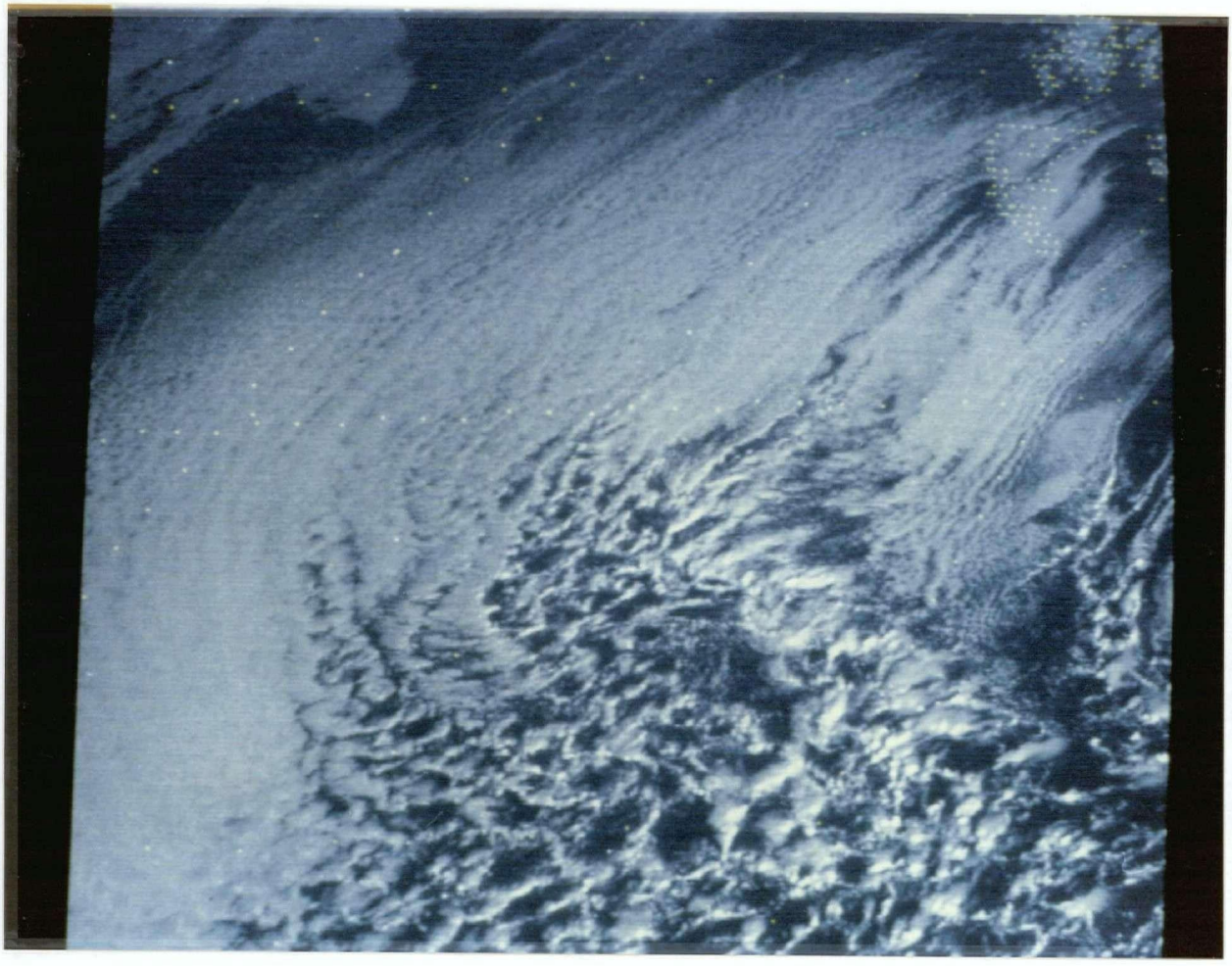

Figure 2.3: 16 February 1989, 18:00Z, visible channel

(1982) compared low level cloud motion winds from various operational systems with numerical model winds, they found errors, calculated from the difference between the cloud data and the 0 hour numerical model data. Their errors for low level cloud motion winds were 4 to 5ms^{-1} for American systems, 7 to 8ms^{-1} for European systems, and 6ms^{-1} for Japanese systems. In contrast, radiosondes have an accuracy of 2 to 3ms^{-1} for low level wind measurements.

For this project, tracking is done using the sequential similarity detection algorithm (SSDA) developed by Barnea and Silverman (1972). This technique is used in the NASA Marshall Space Flight Center system (Wilson, 1984). It was chosen because of its operational success, and because the method was easy to implement. In the first image, at time t, a segment of the image is defined as the template. In the second visual image, at time t + τ, the template is compared to every possible location within a search area. At every location, the sum of the absolute difference between the template pixels and corresponding search area pixels is calculated. The location of the template in the second image is taken to be the location at which the sum is minimum. Wind speed and direction is calculated from the displacement between the original location of the template at time t and the new location at time t + τ. For this study, the SSDA system is semiautomatic. The locations of the template and the search areas are selected by the operator after they have looked at the images a number of times.

The template size, which is 25 by 25 pixels (approximately 30 x 30km at 50°N), is large enough to contain a cloud target and the surrounding clear areas. The search area (75 by 75 pixels) matches the expected velocity scale (approximately 20ms^{-1}).

2.1.3 Wind Estimation

Once the cloud parcel has been tracked, the cloud motion wind is used to estimate the wind speed and direction at a specific height. For this study, it is assumed that the

tracked clouds are passive tracers of the wind that move at the speed of the ambient wind at the cloud base. While not all clouds are passive tracers of the wind, studies by Hasler et al (1979), who collected atmospheric wind velocities at various levels within and below cumulus clouds using an aircraft and then compared these winds with clouds' displacements measured by satellite imagery, indicates that clouds are advected passively by the wind. The study found that in the absence of a vertical wind shear, a cell moves at the ambient wind speed. If there is a shear, then a cell moves at the speed at the cloud base. The height at which to assign cloud motion vectors calculated for open hexagonal cells will be discussed further in section 3.4.

2.1.4 Sources of Error in Estimating Winds from Cloud Motion Wind

There are two principal sources of errors which arise from estimating winds by measuring cloud motions on geostationary satellite imagery. First, errors result from the assumption that all targetted clouds are passive tracers and that measuring the motion of a cloud is the same as measuring the large scale horizontal wind field. Not all clouds are passive tracers of the wind. Clouds with horizontal organization, such as cloud streets, can move at a phase speed that is different than the wind speed. Clouds can be stationary when formed in the updraft caused by gravity waves or flow over mountains. In general however, low level cumulus clouds are considered to be passive tracers of wind at the level of their base. Errors also result because of the uncertainty of the height at which the cloud motion vector should be assigned. The height assignment problem is investigated in Chapter 3.

The second type of error is systematic instrument error. For this study, clouds are tracked using data at intervals of 30 minutes. At $50°N$, the center of the study area, the resolution of the GOES visible images is approximately 1.5km^2. Thus, the maximum obtainable resolution is $1.5\text{km}/30\text{minutes} = 0.8\text{ms}^{-1}$. There is an apparent motion of

stationary objects because of satellite motions. The METDAS system used in this study applies the satellite orbit and attitude information to correct for these registration errors. The images used were also inspected to confirm that there was less than a 1 pixel shift in the relative location of fixed points over a sequence of images. Assuming a 1 pixel shift, registration errors account for an uncertainty of 0.4ms^{-1}.

Algorithm errors occur if a cloud parcel is not tracked correctly. The NASA Marshall Space Flight Center system (Wilson, 1984) had an intermediate quality control designed to reduce this type of error. Two quality control values were calculated:

$$TMQ1 = \frac{SSDA\ mean}{SSDA\ minimum} \tag{2.3}$$

$$SSM = \frac{SSDA\ minimum}{SSDA\ secondary\ minimum} \tag{2.4}$$

where for each possible location of the template in the search area, the difference between the template and search areas is calculated:

$$SSDA = \sum_{for\ all\ pixels} (abs(template\ pixel - search\ area\ pixel)) \tag{2.5}$$

Here $SSDA\ mean$ is the mean value of $SSDA$ over all possible locations of the search area; $SSDA\ minimum$ is the minimum value calculated; $SSDA\ secondary\ minimum$ is the minimum value of $SSDA$ outside the 3x3 array surrounding the location of the $SSDA\ minimum$. The first quantity, $TMQ1$, is a measure of how large a difference there is between the best match, when $SSDA = SSDA\ minimum$, and the average match in the search area, for which $SSDA = SSDA\ mean$. Values of $TMQ1$ close to 1 implies that there is very little difference between the best match and every other possible match. The second quantity, SSM, measures the uniqueness of the match. Large values of SSM imply that other matches, away from the location of $SSDA\ minimum$ may also be the location of the cloud target in the search area. In the NASA system, any vector with

with $TMQ1 < 1.6$ or $TMQ2/TMQ1 \geq 0.88$ was rejected. In the NASA criteria, 96% of the vectors collected for this study were rejected because they failed the second criteria.

Instead of using the NASA method, which rejected many vectors with speeds and directions representative of the mean flow, a vector was discarded in this study when it was more than two standard deviations from the mean direction or mean speed of all vectors collected for a time period. Given the null hypothesis that the observed vectors are normally distributed random variations about a single mean speed and direction, the chance of a valid observation being more than two standard deviations from the mean for a Gaussian distribution is less than 5%.

Over a large region, where the speed and direction of the winds vary considerably, this null hypothesis would not be suitable. However, for this study, the observed flow was homogeneous in the regions where vectors were collected. To test this rejection criterion, a meteorologist independently rejected any vector that was not consistent with the synoptic situation. The same vectors were rejected subjectively as were rejected by the objective criteria.

In all, 12% of the vectors collected were rejected. This is a much higher rejection rate than the 1% of cloud motion vectors that required manual editing in the NASA system (Wilson, 1984). However, there is no report on how many vectors were rejected at their intermediate quality control step.

2.2 Buoy Data

Surface wind speed, wind direction, and wind gust were collected by a set of 9 moored buoys off of the west coast of British Columbia (see figure 2.4). A summary on the buoy data is given in table 2.1. In later sections, buoy data will be referenced by the buoy number (e.g. 46002).

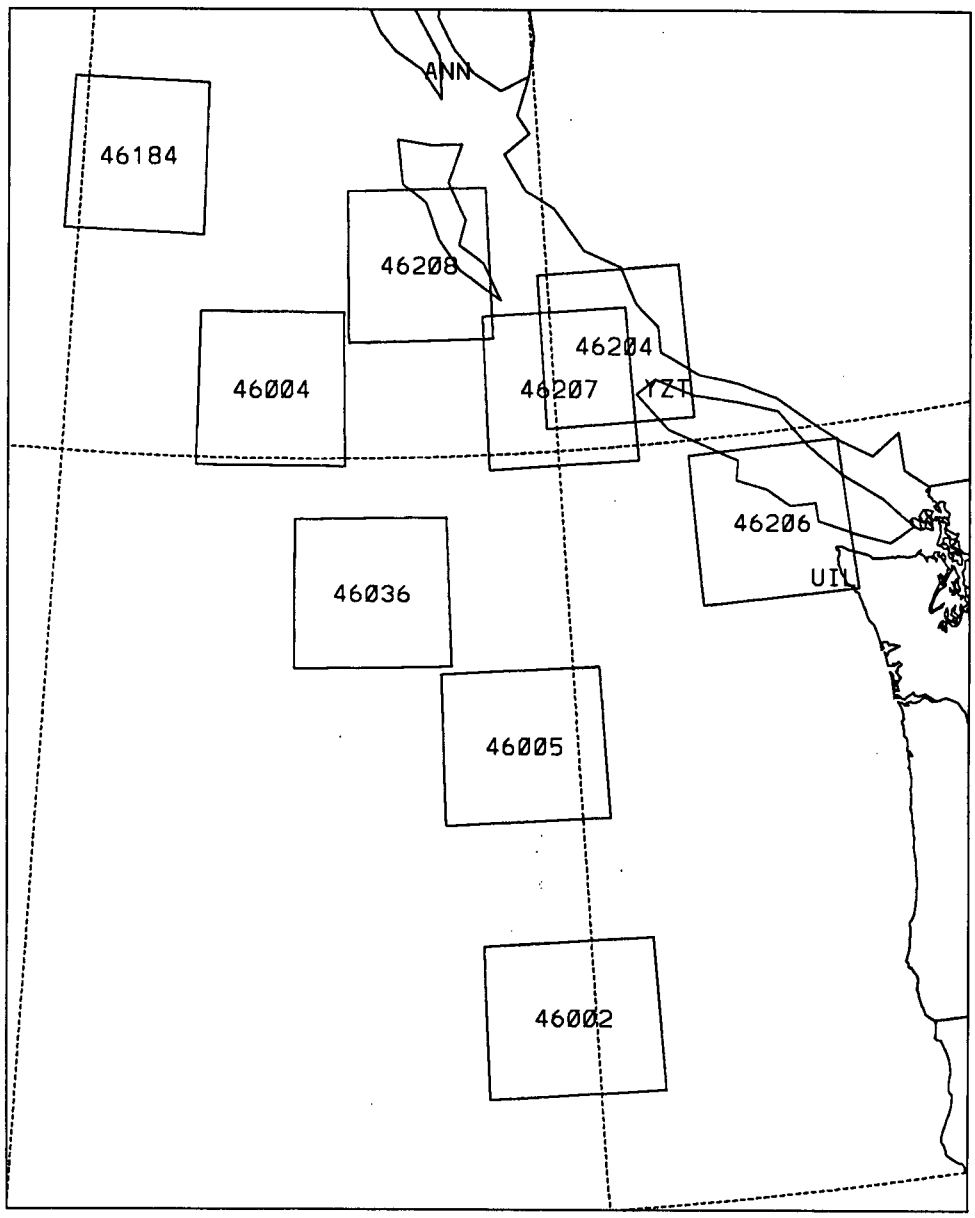

Figure 2.4: Location of moored buoys off of the west coast of British Columbia. Around each buoy is a 2° latitude by 3° longitude box centered at the buoy. The locations of three upper air radiosonde stations: Annette Island, Alaska (ANN), Port Hardy, B.C. (YZT), and Quillayute, Washington (UIL) are also shown.

BUOY	LOCATION Latitude Longitude	BUOY TYPE	HEIGHT OF ANEMOMETER	START OF SAMPLING	END OF SAMPLING
46002	42.5N 130.4W	6 m nomad	N/A	N/A	N/A
46004	50.9N 135.8W	6 m nomad	N/A	00:31	00:41
46005	46.1N 131.0W	6 m nomad	N/A	N/A	N/A
46036	48.2N 133.8W	6 m nomad	4 m	00:30	00:40
46184	53.9N 138.8W	6 m nomad	5 m	00:32	00:42
46204	51.3N 128.7W	3 m discus	4 m	00:46	00:56
46206	48.8N 125.9W	3 m discus	5 m	00:14	00:24
46207	50.8N 129.9W	3 m discus	5 m	00:47	00:57
46208	52.5N 132.7W	3 m discus	5 m	00:48	00:58

Table 2.1: Summary of buoy data

There are two types of buoys: the 6 meter Nomad, and the 3 meter Discus. Both are manufactured by the National Data Buoy Center (NDBC) of the U.S., and contain equipment that meet the same specifications. Each buoy has two anemometers mounted 4 and 5 meters above the buoy deck. For each buoy, only one of the anemometers is used. The height of the anemometer for each buoy is given in table 2.1. The deck is approximately 1 meter above the water.

The wind anemometer, Model 05103 manufactured by the R.M.Young Company, meets the following specifications (the prop measures speed, and the vane measures direction):

Threshold: prop -.3ms^{-1}, vane - 1.0ms^{-1}

Prop accuracy: $\pm$0.3ms^{-1} for speeds $<$ 20ms^{-1}, $\pm$2% for speeds $>$ 20ms^{-1}

Vane accuracy: $\pm$10°

Vane resolution: 1°

Vane dead zone: 0 to 5°

Maximum wind: 60ms^{-1}, short bursts to 80ms^{-1}

Although the vane is accurate to ±5° before deployment, meteorologists at the Pacific Weather Centre consider it accurate only to ±10° because of compass and alignment errors when it is on the buoy (McLaren, 1990).

The wind values were collected once an hour by sampling over a 10 minute interval. in the interval. The data is reported as the next hourly synoptic report. Each buoy has a different data acquisition time (see table 2.1).

2.3 Comparison of the Two Data Sets

In chapter 4, the cloud motion wind data set and the buoy data set will be combined in order to study the relationship between wind estimates from cloud motions and surface winds. Buoy reports will be compared to cloud motion wind reports that satisfy the collocation criteria used by Eriksson (1986) in her comparison of cloud motion wind reports and collocated radiosondes. The criteria are:

Time: Cloud motion wind report within ±1.5 hours of buoy report. Synoptic scale changes in the wind field are not expected to occur in a time period less than 3 hours. At the PWC, meteorological measurements taken in a three hour interval are routinely incorporated into the same forecast.

Location: Cloud motion wind report within a 2° latitude by 3° longitude box centered at the buoy. At 50°N, a 2° by 3° box is 222km from north to south and 214km from west to east. Figure 2.4 shows the area of comparison around each buoy. Comparisons between reports separated by greater than 100 km is not recommended by Gilhousen (1987), who compared moored buoy wind reports with satellite-based scatterometer reports. He compared winds of buoys 109km apart, and found that

the standard deviations of both speed and direction were approximately 3.5 times greater than winds measured by two sensors at the same location. Buoys separated by 40km had standard deviations 2 to 3 times greater than winds measured by sensors at the same location.

Height: Cloud motion wind report for open hexagonal cells. This criteria differs from Eriksson's, who compared only cloud motion winds and radiosonde winds that were within ±50mb. The open hexagonal cells are assumed to have their tops at the top of the boundary layer, which is the lowest 0.5 to 3.0km of the atmosphere. While winds above the boundary layer are geostrophic, within the boundary layer the frictional drag of the ground on the air moving above it modifies the wind. Boundary layer winds are explained further in Chapter 4.

Chapter 3

Cloud Motion Wind Heights

3.1 Introduction

The vector of a tracked cloud is used to estimate the wind at a specific level. Ideally, the cloud motion wind is assigned to the height for which the vector best matches the environmental wind. Realistically, finding the correct height is very difficult. In reviewing 25 years of studies in estimating winds from cloud motion, Isaacs (1986) found that height estimation is the largest source of error when measuring winds from cloud motions.

The purpose of this study is to compare cloud motion winds for open hexagonal cells with surface buoy reports. This chapter explores various methods for determining the height at which to assign the cloud motion winds for these types of clouds. The overwhelming choice of both operational forecasters and researchers (e.g. Wilson, 1984; Isaacs,1986) is to use infrared satellite images to estimate the cloud motion wind height. This method has 2 steps:

- Calculation of the cloud top temperature of the tracked cloud from the measured infrared radiance satellite image.
- Estimation of the cloud motion wind height based on this cloud temperature and a representative vertical temperature profile.

3.2 Cloud Top Temperatures

The first step of calculating the cloud motion wind height is to calculate the cloud top temperature. Noncirrus clouds - cumulus and stratus - radiate as blackbodies, as does the sea surface. If there is no atmospheric absorption or emission between the top of the cloud and the satellite sensor, then the blackbody temperature of a completely noncirrus cloud filled pixel location is the cloud top temperature. If the pixel is completely clear, the blackbody temperature is the sea surface temperature. For the partially filled pixels, the blackbody temperature is a weighted average of the cloud top temperature and the sea surface temperature.

The blackbody temperature is calculated from the infrared pixel value. The GOES 12μm infrared pixel value is converted to a temperature using the following method (Menzel, 1984). First, the 8 bit pixel value is converted to a monochromatic radiance with respect to wavenumber (i.e. for the 12μ wavelength):

$$R = (AP - B) \text{ mW m}^{-2} \text{ str}^{-1} \text{ cm} \tag{3.6}$$

where R is radiance, $A = 0.96$, $B = 10$, and P is the 8 bit pixel value.

Then the radiance is converted to a blackbody temperature using Planck's law:

$$T = (\frac{PK2}{log(PK1/R + 1)} - TC1)/TC2 \tag{3.7}$$

where the constants for the infrared window are

$$PK1 = 8438 \text{ mW m}^{-2} \text{ str}^{-1} \text{ cm}$$

$$PK2 = 1283^{\circ}K$$

$$TC1 = 0.3263^{\circ}K$$

$$TC2 = 0.9973(unitless)$$

This conversion accounts for the spectral response characteristics of the infrared window bandpass filter on GOES-6.

Having determined how to calculate the blackbody temperature for any given pixel, the problem of choosing the pixels to be used remains. For this study, a cloud element in a 25 by 25 pixel box is tracked. Some of the pixel locations will be completely filled, some will be partially filled, and some clear. Figure 3.1 shows the histogram for the minimum blackbody temperatures for all of the clouds tracked on 24 November 1989 and 16 February 1990. The wide range of temperatures is not what would be expected if these were all values of the cloud tops. All of the clouds that were tracked were open hexagonal cells, which implies that the cloud tops were at a uniform level. Therefore, we would expect the cloud top radiative characteristics to be homogeneous: all of the clouds should have the same cloud top temperatures. Because there is a wide range in temperatures, some of the minimum temperature pixels of the tracked clouds must be only partially cloud filled, or be contaminated by overlaying cirrus. This is shown by an example taken from 16 February 1990. Figure 3.2 shows a visible subimage taken on this day. In these images, low albedo values (clear sky) are brighter, and high albedo values (clouds) are darker. Figure 3.3 is the infrared subimage for the same region. Low (cold) infrared pixels are bright, while high (warm) infrared pixels are dark. Area A contains a hexagonal cell with a 70km diameter and cloud walls from 11 km thick at 1 and 18 km thick at 2. On side B , the minimum blackbody temperature is $-15°C$, while on side C the minimum is $-7°C$. In a dry atmosphere, the air would be cooled at a rate of $9.8°C$ for every kilometer it ascends assuming this cooling occurs adiabatically. In a saturated atmosphere, the latent heat released by condensing water would offset this rate of cooling, resulting in a lapse rate between 6 and $7°\text{Ckm}^{-1}$. For open hexagonal cells, Agee and Dowell (1974) have measured a mean lapse rate of 8°Ckm−1. If the two cell sides both had cloud filled pixels, then the temperature difference observed between

the two sides would correspond to an approximate a 1km difference in elevation. Since sides B and C have approximately the same height, the marked difference in the cloud top temperatures on the two sides must occur because there are no cloud filled pixels on side C. In area D, the visible pixels are brighter than the clear pixels in the centers of the hexagonal cells but not as dark as the pixels that make up the walls of the open hexagonal cells. This, along with the fact that the temperature of the area is $-18°C$ indicates the presence of cirrus.

The next section investigates possible methods for selecting cloud filled pixels for open hexagonal cells given the problems caused by partially filled pixels and overlaying cirrus.

3.3 Selection of Cloud Filled Pixels

A technique developed by Coakley and Bretherton (1982) was used to investigate the distribution of cloud filled, partially filled, and clear pixels. Coakley and Bretherton studied the distribution for a scene containing only one layer of clouds. The input of their study was global area coverage (GAC) data constructed from $11\mu m$ Advanced Very High Resolution Radiometer (AVHRR) data. The $1km^2$ resolution AVHRR data is resampled as follows: For each set of three scan lines, the first line is sampled. Along the first scan line, 4 adjacent pixels were averaged. Then the next pixel is discarded. This pattern is repeated for the entire scan line. The second and third lines were discarded. The resolution of the GAC data is approximately $5x3km^2$.

The local mean blackbody temperature and local standard deviation of every 8x8 box in the image was calculated. Coakley and Bretherton found that an arch structure with two feet was formed when the mean and standard deviation values were plotted for an image with a single cloud layer. In figure 3.4, the image is divided into 16 sections, and the mean and std values are plotted. The radiating characteristics of the cloud tops of

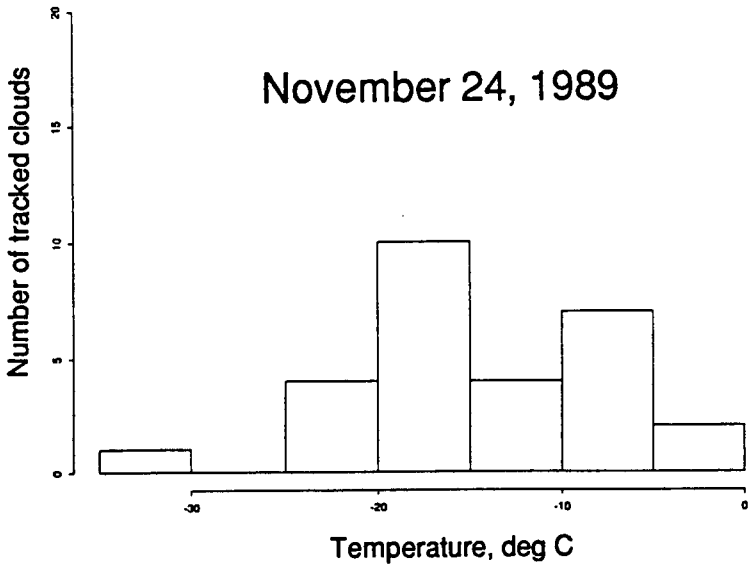

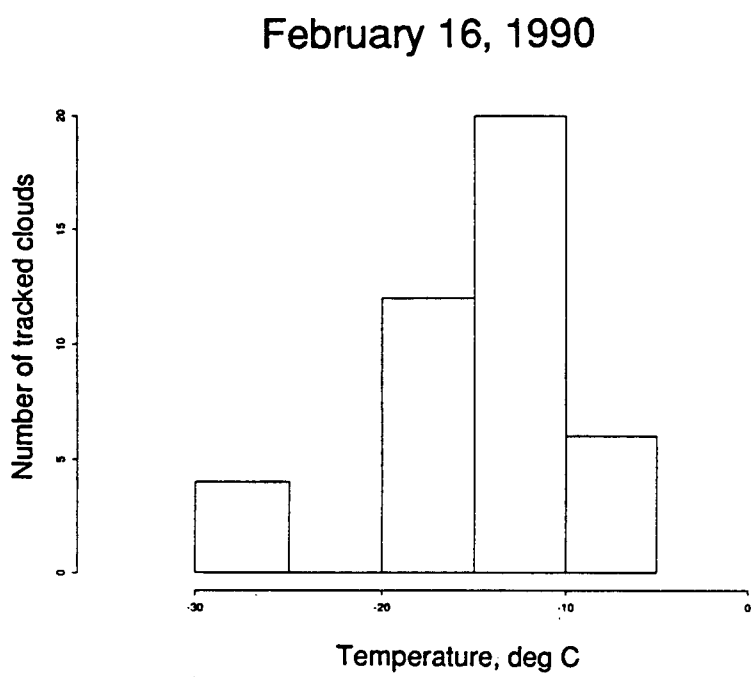

Figure 3.1: Histogram of minimum blackbody temperature for all clouds tracked on 24 November 1989 and 16 February 1990.

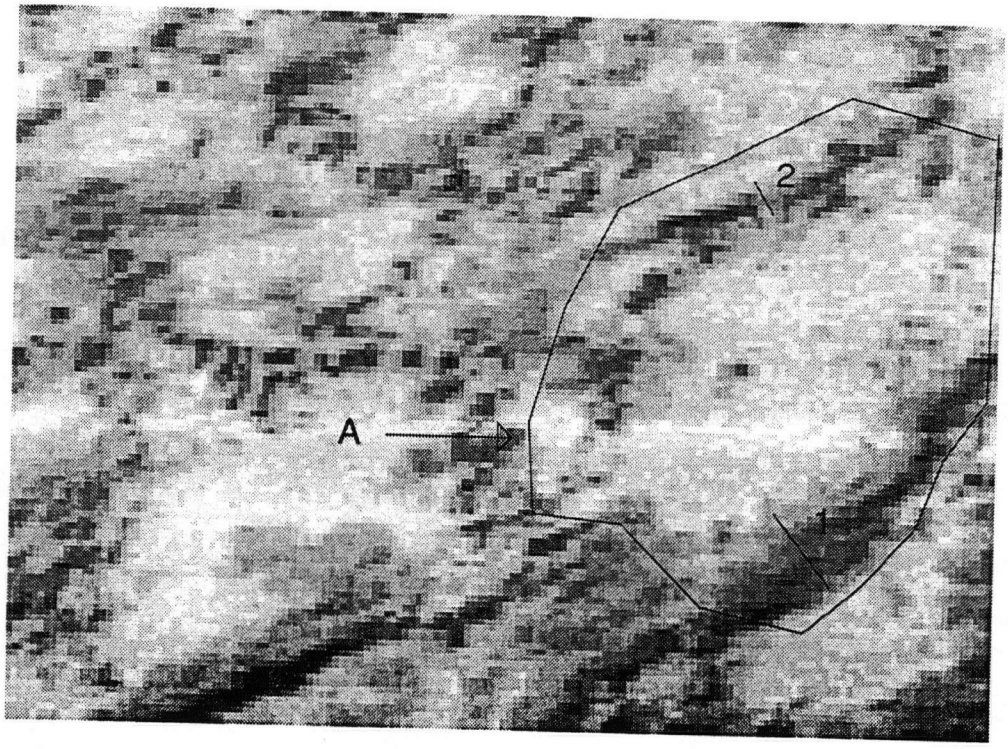

Figure 3.2: 16 February 1990, 17:30Z, visible channel, subimage, lines 741-863, pixels 356-512, with labels. Cell A is a cell 70 km wide, with cell wall 18 km thick at 1 and 11 km thick at 2. Dark pixels are cloudy, bright pixels are clear.

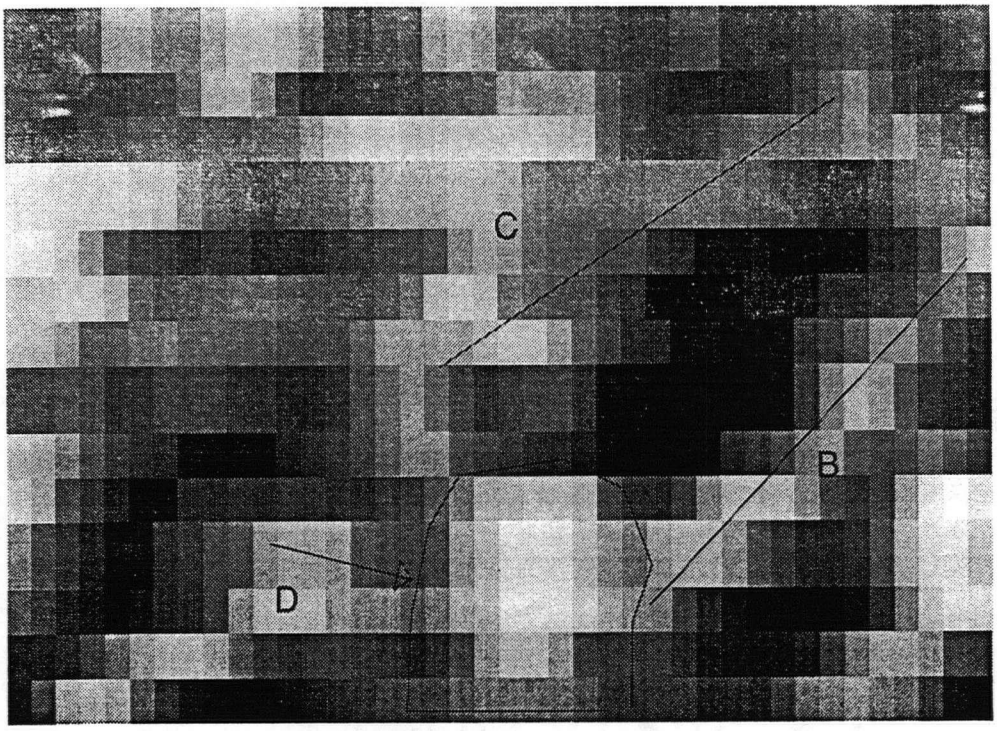

Figure 3.3: 16 February 1990, 17:30Z, infrared channel, subimage. Side B has a minimum temperature of $-15°C$. Side C has a minimum temperature of $-7°C$. Area D is cirrus, with a a temperature of $-18°C$. Dark pixels are clear, bright pixels are cloudy.

a layer of cloud are homogenous, as are the radiating characteristics of the sea surface. Regions that are totally cloud filled have a uniform low temperature and low standard deviations. Pixels in these regions form the left foot. Regions that are clear have uniform high temperatures and low standard deviations. Pixels in these regions form the right foot. At the cloud edges, between cloudy regions and clear regions, the pixel locations are partially filled. The temperature of these partially-filled pixel locations are an average of the colder cloud-top temperature and the warmer sea surface temperature. At the cloud edges, the standard deviations are high: the standard deviation is a crude edge detector. The partially filled pixels form the center of the arch.

Figures 3.5 and 3.6 are the diagrams obtained for 16 February 1990 and 24 November 1989, using Coakley and Bretherton's technique. In this case, the input was GOES 12μm infrared imagery which has a 32km^2 spatial resolution at satellite nadir (4km along a line and 8km between lines). To maintain a sample area having equivalent spatial coverage to that used by Coakley and Bretherton, the local mean blackbody temperature and local standard deviation are calculated for every 10 pixel by 3 line box. Larger and smaller boxes were tried, and yielded similar results. The local mean blackbody temperature and local standard deviation are plotted for the 16 subimages shown in figures 3.7, 3.8.

As seen on figure 2.3, on 16 February, there were two major types of cloud: cloud streets spaced at 7km intervals, and open hexagonal cells with diameters from 20 to 96km. There was almost no cirrus in the entire image. For the parts of the image that contained cloud streets and open water (figures 3.5 (b), (c), (d), (e), (f), (g), (h), the arch structure is fairly well defined. Clear pixels form the first foot at about 0°C. Cloud filled pixels form a second foot at -16°C. In subimages (i) and (m) have cold feet at -16°C, but because of the lack of clear pixels, neither has warm feet. For the areas of the image that contained open hexagonal cells ((j), (k), (l), (n), (o) and (p)), only (j) has a foot at -16°C, which is formed because of the presence of some cloud streets in (j).

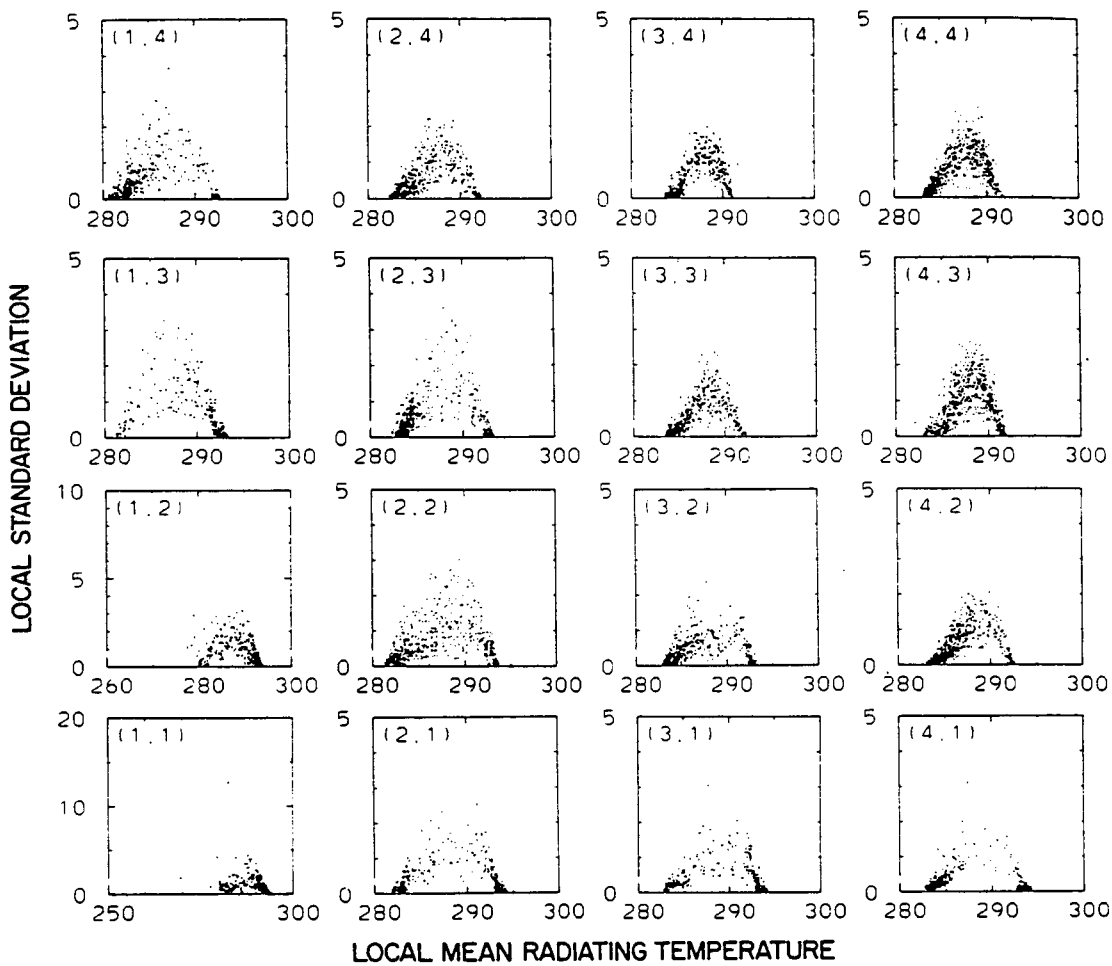

Figure 3.4: The 11μm local mean blackbody temperatures and local standard deviations for 8x8 arrays of GAC data points constructed for a scene centered at 22.3°N, 136.7°W, on June 7, 1979, at 1500 LT. The cluster of points near 293 K represents cloud-free pixels; the cluster near 283.5 K represents cloud-covered scan spots. The points between these clusters represent partially covered fields of view. Coakley and Bretherton (1982).

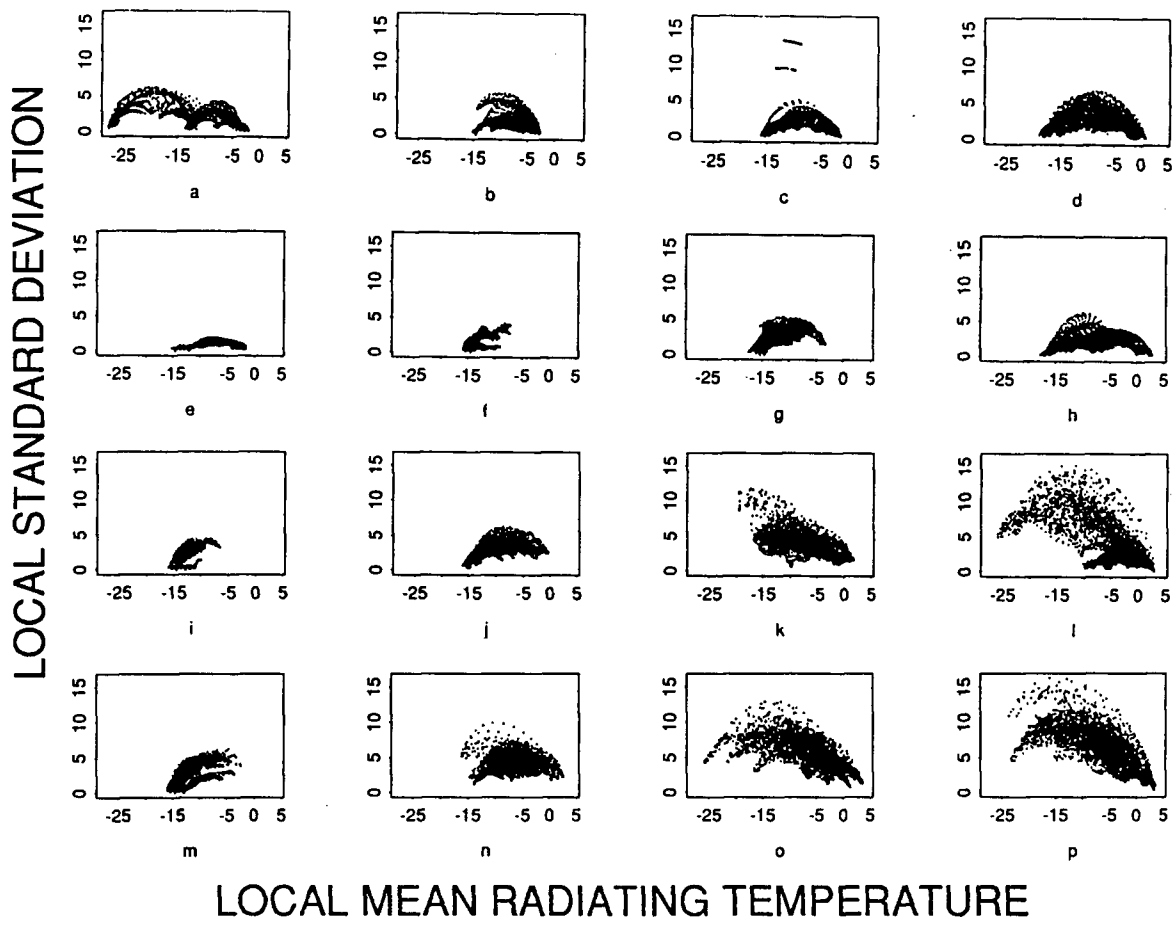

Figure 3.5: The 11μm local mean blackbody temperatures and local standard deviations for 10x3 arrays of GOES data points constructed for a scene centered at 49.0°N, 134.0°W, on 16 February, 1990, at 17:30Z

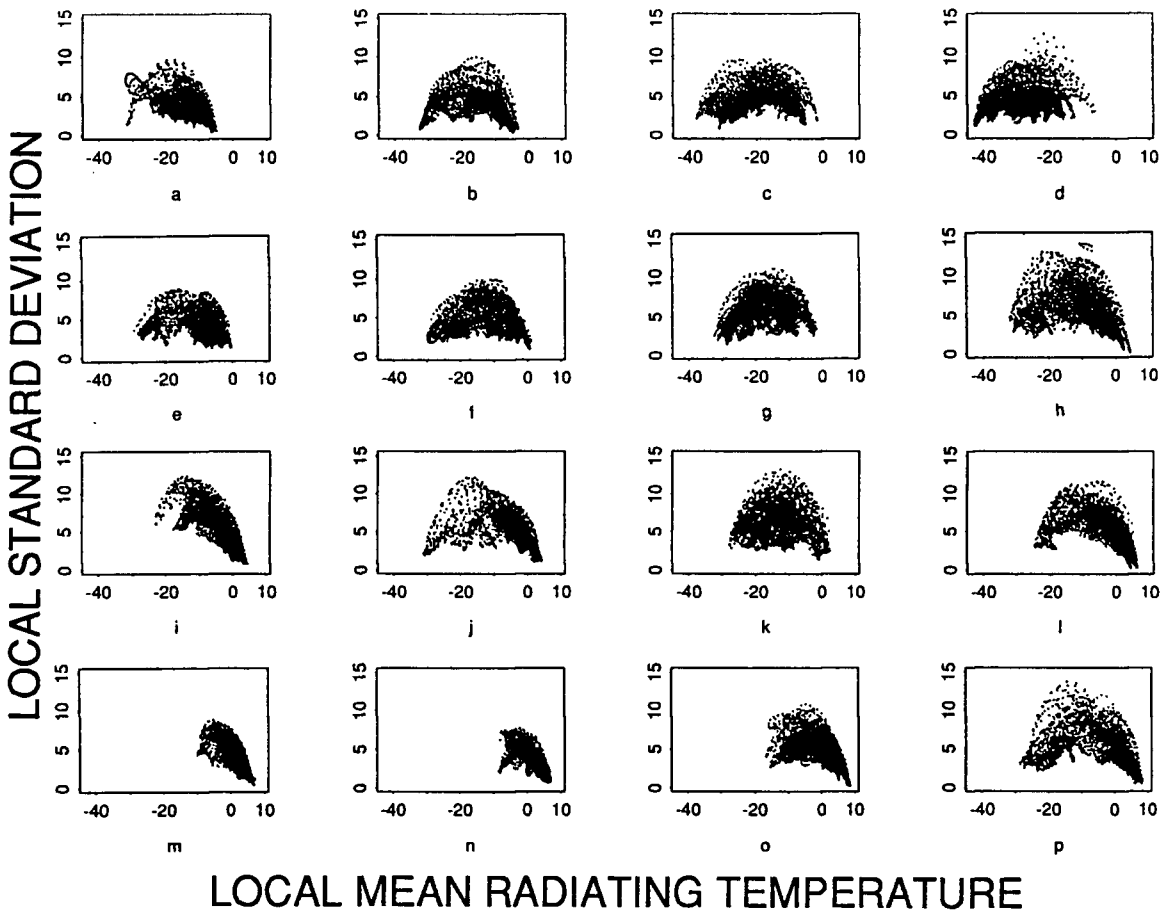

Figure 3.6: The 11μm local mean blackbody temperatures and local standard deviations for 10x3 arrays of GOES data points constructed for a scene centered at 50.0.3°N, 135.0°W, on 24 November 1989, at 18:00Z

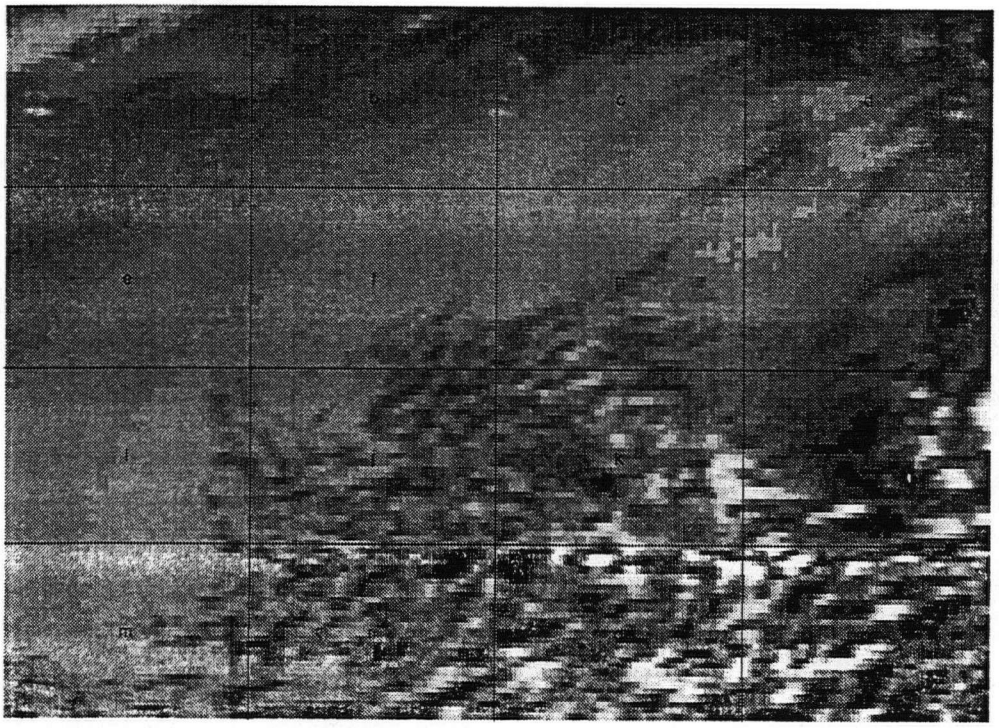

Figure 3.7: 16 February, 1990, at 17:30Z: Location of 16 subimages. Dark pixels are warm, bright pixels are cold.

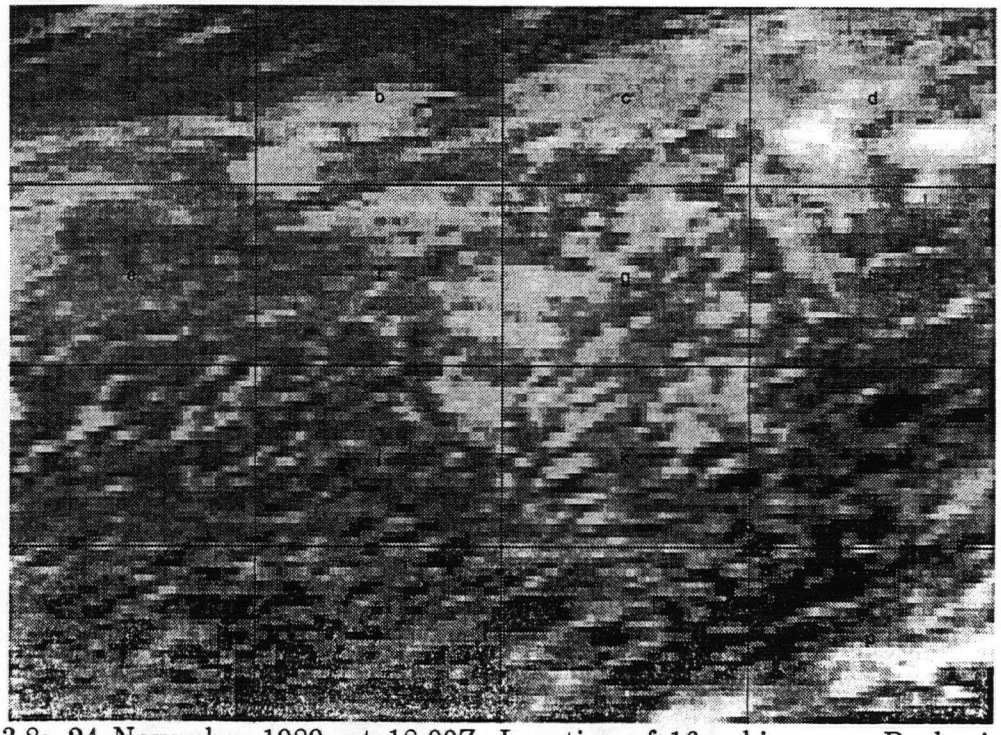

Figure 3.8: 24 November 1989, at 18:00Z: Location of 16 subimages. Dark pixels are warm, bright pixels are cold.

For the others ((k), (l), (n), (o) and (p)) clear pixels form the first foot at approximately 4°C. There is no second foot, but instead, there are a series of multiple arches which are formed because of the presence of cirrus.

In determining the correct cloud top temperature to use for the open hexagonal cells, it is useful to remember that the air mass that contains these cells is the same that contains the cloud streets. It can be expected that the cloud heights of the two cloud types are at approximately the same level. Therefore, −16°C is the appropriate temperature to use when estimating the height at which to assign the cloud motion wind.

On 24 November, shown in figure 2.1, the image contained open cells ranging in size from 20 to 115km in diameter. Determining the cloud top temperature of these open hexagonal cells is more difficult because cirrus overlay the cells in most of the image except the lower left quadrant. Often, a threshold method is used to establish the temperature of low-level cloud tops when cirrus contamination is present. Since dry cools adiabatically at more than 9.8°Ckm^{-1} and moist air cools at even lower rates, cloud tops below 3km cannot be more than 30° colder than the underlying surface temperature. Therefore, if the sea surface temperature is 10°C, a threshold of −20°C would eliminate pixels measuring clouds above 3km. However, the threshold method is not satisfactory in eliminating those pixels with partial cirrus contamination. It is difficult to determine the correct threshold value. While open hexagonal cells are typically below 3km, their heights can range from 1 to 4.5km, with corresponding temperature differences with the surface of 8 to 36°C assuming a mean lapse rate for open hexagonal cells of 8°Ckm^{-1} (Agee and Dowell, 1974).

Figure 3.9 is histogram of temperature for the 16 subimages on 24 November. Although there is a well defined peak, at 8°C for the sea surface temperature, there is no peak for the open cell cloud top temperature in subimages (i), (j) (m), and (n). Instead, there is a gradual decrease from the sea surface temperature peak down to a minimum

of from $-36°C$ for subimage (j), to $-15°C$ for subimage (n). Since the cloud top temperature of the open cells is homogeneous, this range in values is caused by partially filled pixels. In addition, the coldest pixels in each subimage must either contain some cirrus or be only partially filled. Otherwise, all four regions would have the same minimum temperature. Because there is no peak on the histogram corresponding to the temperature of completely low-level cloud filled pixels, and there is cirrus contamination the appropriate threshold temperature could not be chosen.

The Coakley/Bretherton diagram for 24 November, figure 3.6, offers a possible alternative method for determining the cloud top temperature of the open cells. The high, wide arches, in all but subimages (m) and (n), indicate the presence of cirrus. Unlike the February case, where the cirrus only formed arches with a warm foot, but no cold foot, for this case the large amounts of cirrus resulted in a foot at -20 to $-42°C$. Without large amounts of overlaying cirrus, the open hexagonal cells and the water below in subimages (m) and (n) formed arches with warm foot near $8°C$, and a cold foot at $-10°C$ for (m) and $-8°C$ for (n). But neither case does the cold foot have as small local standard deviations as found in the February example or in Coakley and Bretherton's original example. As well, these temperatures are averages over an area 10 pixels by 3 lines of the infrared image and are not the temperature of fully filled cloud pixels.

The Coakley/Bretherton technique is well suited for finding the temperature of the cloud tops when the clouds fill large regions. However, because the resolution of the infrared pixels are 4km along a line by 8km between lines, while the the thickness of the open hexagonal cell walls are from 10 to 15km, this technique failed to find the cloud top temperature of the cells. As mentioned previously, computing the local mean blackbody temperature and local standard deviation for smaller regions did not solve the problem. However, the method was successful in finding the temperature for the ocean surface and for cloud streets, which fill much larger regions than the cells. It also detected cirrus, not

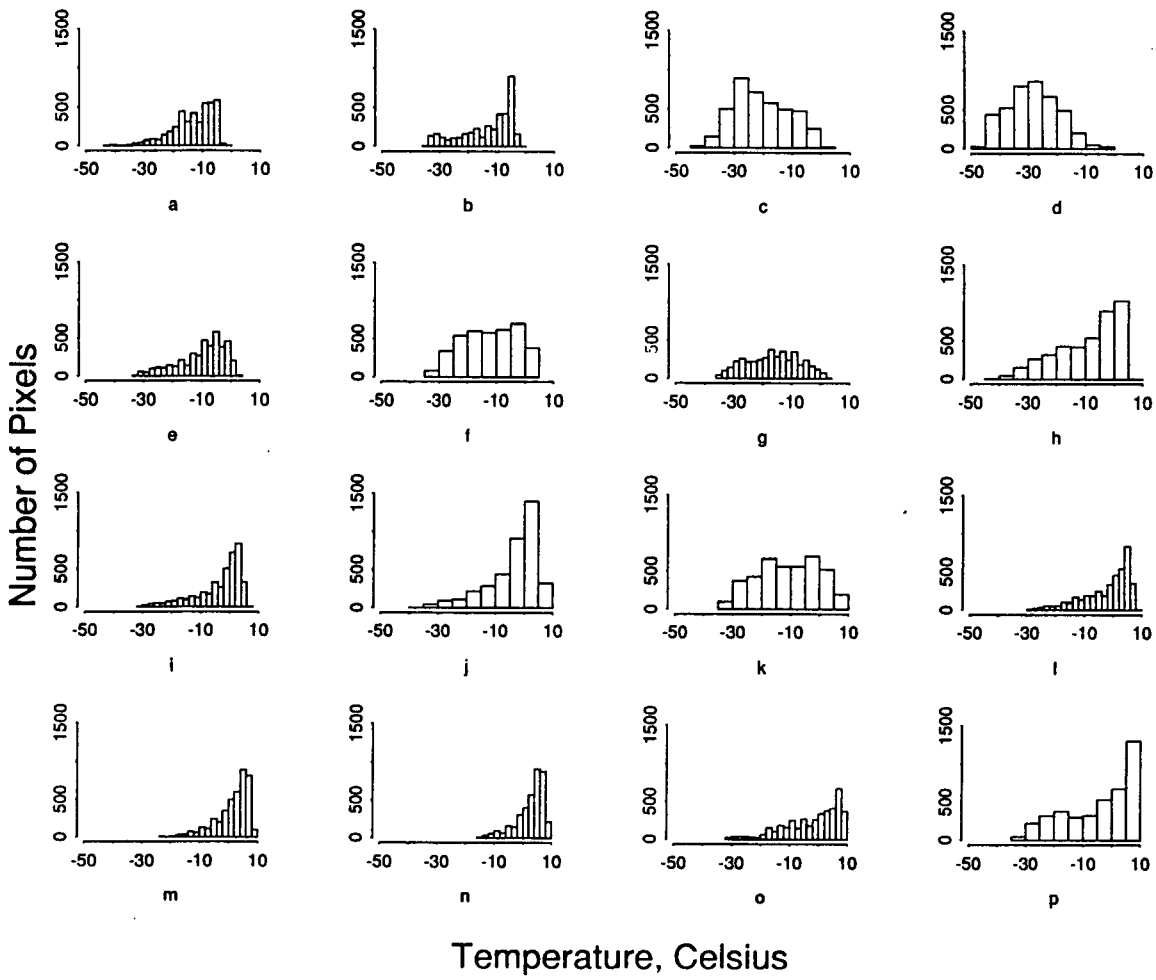

Figure 3.9: 24 November 1989: Histogram of blackbody temperature, in degrees Celsius, for 16 subimages.

only when there was large quantities, such as in November, but when there was small amounts, as in February.

Another approach to finding the cloud top temperature is to use both the visible and infrared images to determine which pixels are most likely to be cloud filled and have no cirrus contamination. For both subimages (m) and (n), the coldest infrared pixel, and brightest pixel that was located on a hexagonal cell wall was found. For (m), the temperature of this pixel was $-15°C$, and for (n), $-18°C$.

3.4 Height Calculation

In this section the cloud motion wind heights are estimated. There are several choices available. Because of the difficulty in estimating heights, many studies simply assign the vectors to low (0 to 2km), medium (2 to 7km) or high (7 to 10km) height (e.g. Wilson, 1984; Isaacs, 1986). Applying this method, all of the tracked open hexagonal cells would be assigned to a low height, since the bases of open hexagonal cells are usually well below 2km, while the tops of the cells rarely exceed 3km (Agee and Dowell, 1974).

A more refined alternative is to assign the cloud motion winds to a specific height as is done in most operational systems. For instance, the U.S. Weather Service assigns all low-level cloud motion winds to 900 mb because the average difference between low-level cloud motion winds and radiosondes has been found to be at a minimum near this level (Hubert and Thomasell, 1979). This level is also statistically close to the average low-level cloud base height over the ocean (Hubert,1979).

Another approach is to estimate the cloud motion wind height from the cloud top temperature and a vertical temperature profile. As mentioned in section 2.1.3, this study assumes the tracked clouds are passive tracers of the wind at the cloud base. While this assumption seems reasonable based on observations (Hasler et al, 1977, 1979), the

drawback is that the height of the cloud base is difficult, if not impossible, to estimate from the visible and infrared satellite measurements. Further, in ocean regions, where cloud motion winds are most often collected, other measures of cloud base height are usually sparse or nonexistent. What can be estimated is the cloud top height by using the cloud top temperature and a representative vertical temperature profile:

$$height = (ctt - sst)/(lapse\ rate) \tag{3.8}$$

where ctt = cloud top temperature, sst = sea surface temperature, and $lapse\ rate$ = the vertical rate of temperature decrease of the air.

Between the ground and the top of the open hexagonal cell, at the top of the boundary layer, the vertical shear of the wind is very weak as momentum from aloft is mixed with the slower air below. For instance, the average shear for 18 cases of open hexagonal cells was $2.3 ms^{-1}km^{-1}$ (Agee and Dowell, 1974). Therefore it is reasonable to assume that there is a minimumal vertical wind shear, and the cloud motion vector effectively represents the wind not only at the base of the cloud, but throughout the entire height of the cloud.

Based on the results of the previous section, the estimates of the cloud top temperatures for open hexagonal cells is $-20°C$ for 24 November 1989 and is $-16°C$ for 16 February 1990. For this study, the vertical temperature profile used will be calculated from observed sea surface temperatures and a mean vertical lapse rate of $8°Ckm^{-1}$. The sea surface temperature is taken from the warmest foot of the Coakley Bretherton diagram. The choice of $8°Ckm^{-1}$ for a mean lapse rate is based on the results of Agee and Dowell's investigations as has beend discussed in section 3.2.

Using this method for calculating the cloud motion wind height, the tracked clouds on 16 February had cloud top heights of 2.5km. In contrast, if the minimum pixel

temperature of the tracked clouds had been used, cloud top height estimates varied from 1.3km to 3.9km with an average of 2.3km. An alternative method of estimating the cloud top height for the February day is to use Weston's (1980) finding that the aspect ratio of the streets is approximately 3. Since the cloud streets are spaced at 7km intervals, the height of the rolls is approximately 2.3km.

For the November day, the cloud top heights are 3.5km. Using the minimum pixel temperature of the tracked clouds, the cloud top height estimates varied from 1.3 to 4.9km with an mean of 2.8km.

Chapter 4

Results

In this chapter, the cloud motion vectors collected for 3 winter days will be compared with surface winds collected at 9 moored buoys. On the first two days, 24 November 1989, and 16 February 1990, open hexagonal cells were tracked. On the third day, 5 January 1990 unorganized cumulus clouds were tracked.

For each day, a number of meteorological charts will be presented:

- subjectively analyzed surface synoptic weather chart
- plots of buoy observed wind data
- objectively analyzed $850mb$ geopotential height contours
- plots of radiosonde observed upper air data
- semiautomatically and manually tracked cloud motion vectors
- collocated cloud motion and buoy winds

The surface synoptic chart is subjectively analyzed by a senior forecaster at the Pacific Weather Center from land, ship and buoy surface synoptic observations. The contours are isobars - lines of equal mean sea level pressure values. The geostrophic wind blows parallel to the isobars. The horizontal gradient of the isobars is proportional to the strength of the geostrophic wind.

The buoy observations show the surface winds at various locations off the west coast of Vancouver Island for the time periods that cloud motion winds were collected. For each of the three case studies, the winds at the buoys were effectively steady in speed and direction over the period that cloud motion vectors were collected.

The geopotential height analysis depicts contours of constant geopotential height at a constant pressure level. The height fields were generated by objective analysis of upper air observations. From this chart, geostrophic winds can be estimated from the geostrophic wind approximation:

$$u_g \equiv -\frac{g_o}{f}(\frac{\partial Z}{\partial y})_p \tag{4.9}$$

$$v_g \equiv \frac{g_o}{f}(\frac{\partial Z}{\partial x})_p \tag{4.10}$$

where u_g and v_g are the zonal and meridional components of the geostrophic wind, $f \equiv 2\Omega \sin\phi$ is the Coriolis parameter, Ω is angular speed of rotation of the earth, ϕ is latitude, g_o is the global mean of gravity at a standard atmospheric mean sea level, $\frac{\partial Z}{\partial x}$ and $\frac{\partial Z}{\partial y}$ are the geopotential height gradients , p is a constant pressure level.

The upper air soundings show the wind observations measured by radiosondes at the coastal stations of Annette Island, Port Hardy and Quillayute (for their locations see figure 2.4). The distance between these station sites and the positions at which clouds were tracked ranges from 300 to 1400km.

The cloud motion vectors were collected by the semiautomatic SSDA method outlined in section 2.1.2. These vectors will be compared with manually tracked cloud motion winds and with upper level wind winds estimated from the geostrophic height charts, and measured at upper air radiosonde stations. The SSDA cloud motion vectors will also be compared with collocated surface buoy wind reports.

From the data that will be presented, along with knowledge on the characteristics

Semi-automatic Cloud Motion Winds	Manual Cloud Motion Winds	Buoy Winds	Geostrophic Winds	Rawindsonde Winds
No. of clouds tracked: 34	No. of clouds tracked : 34	Buoys	Level = 850 mb	Stations
No. rejected: 6	No. rejected: 0	46004	Height= 1.4 km	UIL
Speed (ms^{-1}):	Speed (ms^{-1}):	46005	Speed : 11 to 19ms^{-1}	YZT
Mean 14	Mean 15	46036		
Minimum 8	Minimum 10	46184		Distance from clouds:
Maximum 19	Maximum 21	46206		300 to 1000km
Std.Dev. 3.4	Std.Dev. 3	46207		
		46208		Speed at 1.4km:
Direction (^{o}):	Direction (^{o}):			7 to 12ms^{-1}
Mean 272	Mean 273	Speed:8.2ms^{-1}		Speed at 3.4km:
Minimum 262	Minimum 261	Direction:270^o		7 to 19ms^{-1}
Maximum 282	Maximum 284			
		Time: 11 to 21Z	Time: 12Z	Time: 24 Nov, 12Z
Height of clouds: 3.4km	Height of clouds: 3.4kms			
Time: 17:30 to 18:00Z	Time: 17:30 to 18:00Z			25 Nov, 12Z

Table 4.1: Summary of Data Collected and Analyzed on 24 November, 1989

of open hexagonal cells, and unorganized cumulus clouds, this research finds that the directional components of the cloud motion winds is a reasonable representation of the directional component of the synoptic scale flow. The lack of directional shear between the open hexagonal cells and the surface, and the directional shears of 14° to 27° for the unorganized cumulus clouds are typical of what is expected for the two types of clouds. However, a larger variation in speeds is observed for the open hexagonal cells than would be expected if the cloud motion vectors represented environmental winds at a uniform level.

4.0.1 Case Study - 24 November 1989

A summary of the data for this day is given in table 4.1.

On this day, seen in figure 2.1, between 17:30Z and 18:00Z, 34 cloud targets were tracked using the SSDA scheme. Of 34 vectors collected, 6 were rejected using the criteria outlined in section 2.1.4. The remaining vectors are depicted on figure 4.1. Speeds ranged from 8ms^{-1} to 19ms^{-1} with a mean speed of 14ms^{-1} and a standard deviation of 3.4ms^{-1}. The vectors were westerly, ranging from 262° to 282°, with an mean direction of 272° and a standard deviation of 5.6°.

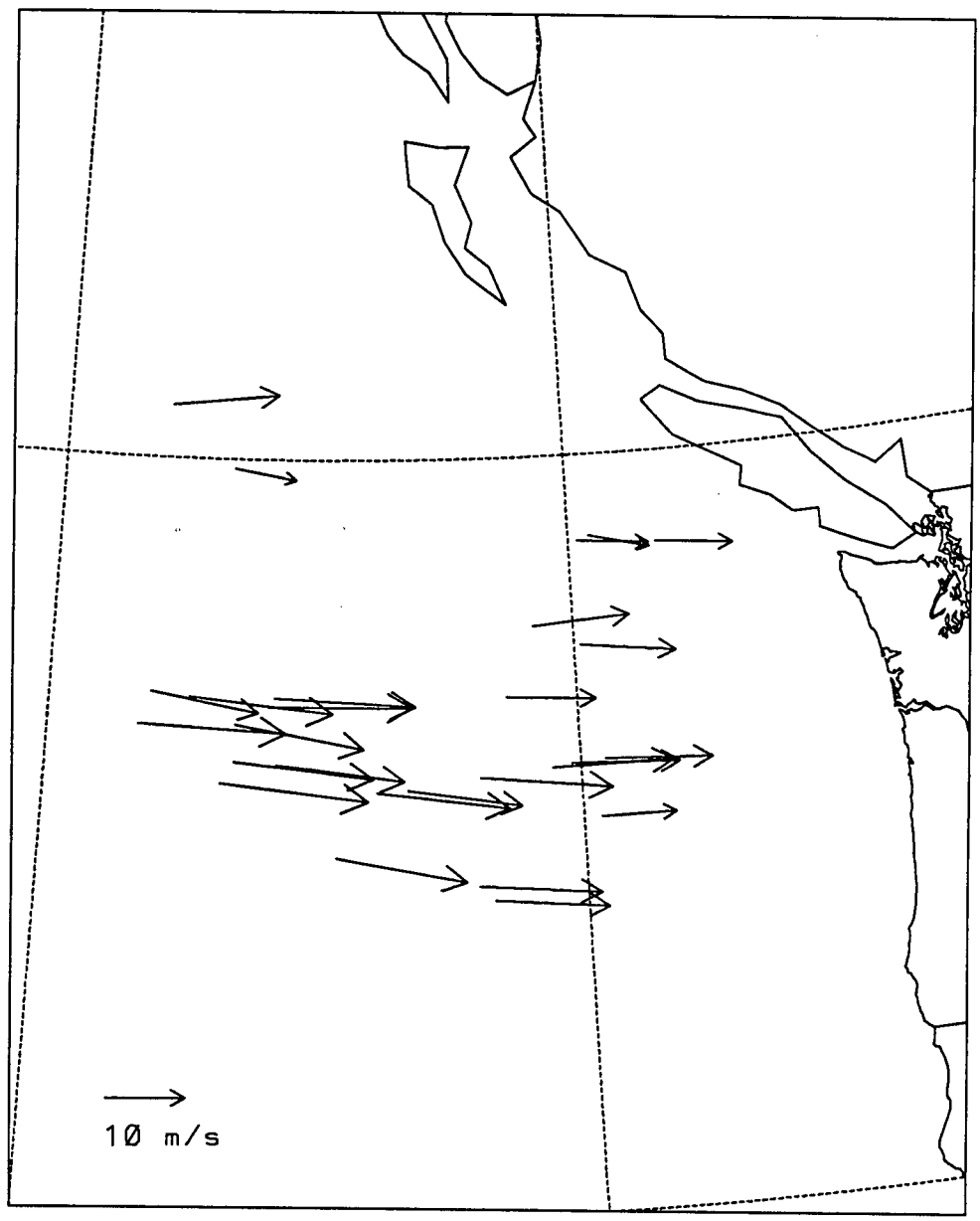

Figure 4.1: 24 November 1989, SSDA tracked cloud motion vectors collected from 17:30Z to 18:00Z

The same 34 cloud parcels were also tracked manually. The manual vectors are shown in figure 4.2. The ranges of values for the speed and directions are almost identical to values for SSDA tracked clouds. Manually tracked cloud speeds were from $10ms^{-1}$ to $21ms^{-1}$, and averaged $15ms^{-1}$ with a standard deviation of $3ms^{-1}$. Directions for the clouds were from 261° to 284°, with an mean direction of 273°. Subjectively, the SSDA and manual vector sets are comparable in depicting the synoptic scale flow.

The geostrophic wind approximation was used to estimate the winds from the $850mb$ geopotential height contours generated by objective analysis for 24 November, at 12:00Z (figure 4.3). In the region where the clouds were tracked, the winds at 850mb, at approximately 1.4km above the ground, were $11 \pm 1ms^{-1}$ to $19 \pm 2ms^{-1}$. These wind speeds agree closely with those collected by tracking the clouds.

Figure 4.4 shows the upper air radiosondes collected at 3 shore stations for 24 November, at 12:00Z and 25 November, at 12:00Z. Quillayute and Port Hardy are downstream from the vector flow. At 1.4km, the level of the $850mb$ pressure level, reported wind speeds at Quillayute were approximately $10ms^{-1}$ for both observation times. The winds decreased from 12 to $7ms^{-1}$ at Port Hardy during the same period. At 3.4km, the estimated height of the open hexagonal cell cloud tops, winds decreased from $19ms^{-1}$ to $13ms^{-1}$ at Quillayute, and from $15ms^{-1}$ to $7ms^{-1}$ at Port Hardy. The stations are 300 to 1000km from the vectors.

Surface winds were collected from 11:00Z to 21:00Z for 7 buoys (46004, 46005, 46036, 46184, 46206, 46207, 46208). As seen from figure 4.5, surface winds during this period were moderate and steady with speeds away from the land averaging $8.2ms^{-1}$ with a standard deviation of $1.8ms^{-1}$. The wind direction was from the west, except at the northern most buoy, 46184, where the surface winds were southwesterly. There was much less coherence in the near shore buoys (46206, 46207, 46208), where topography reduced the wind speed and disrupted the uniform wind direction observed farther offshore. Figure

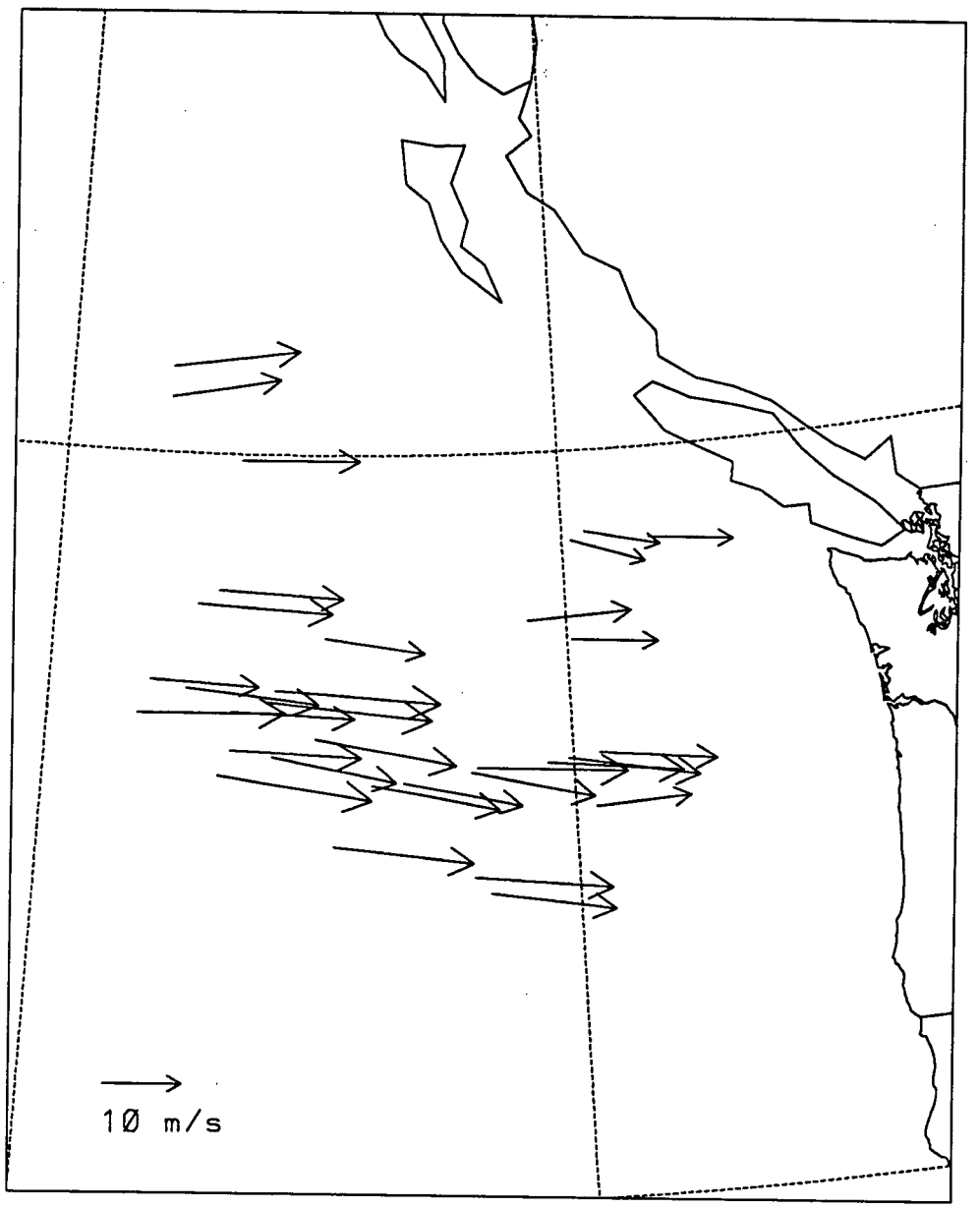

Figure 4.2: 24 November 1989, manually tracked cloud motion vectors collected from 17:30Z to 18:00Z

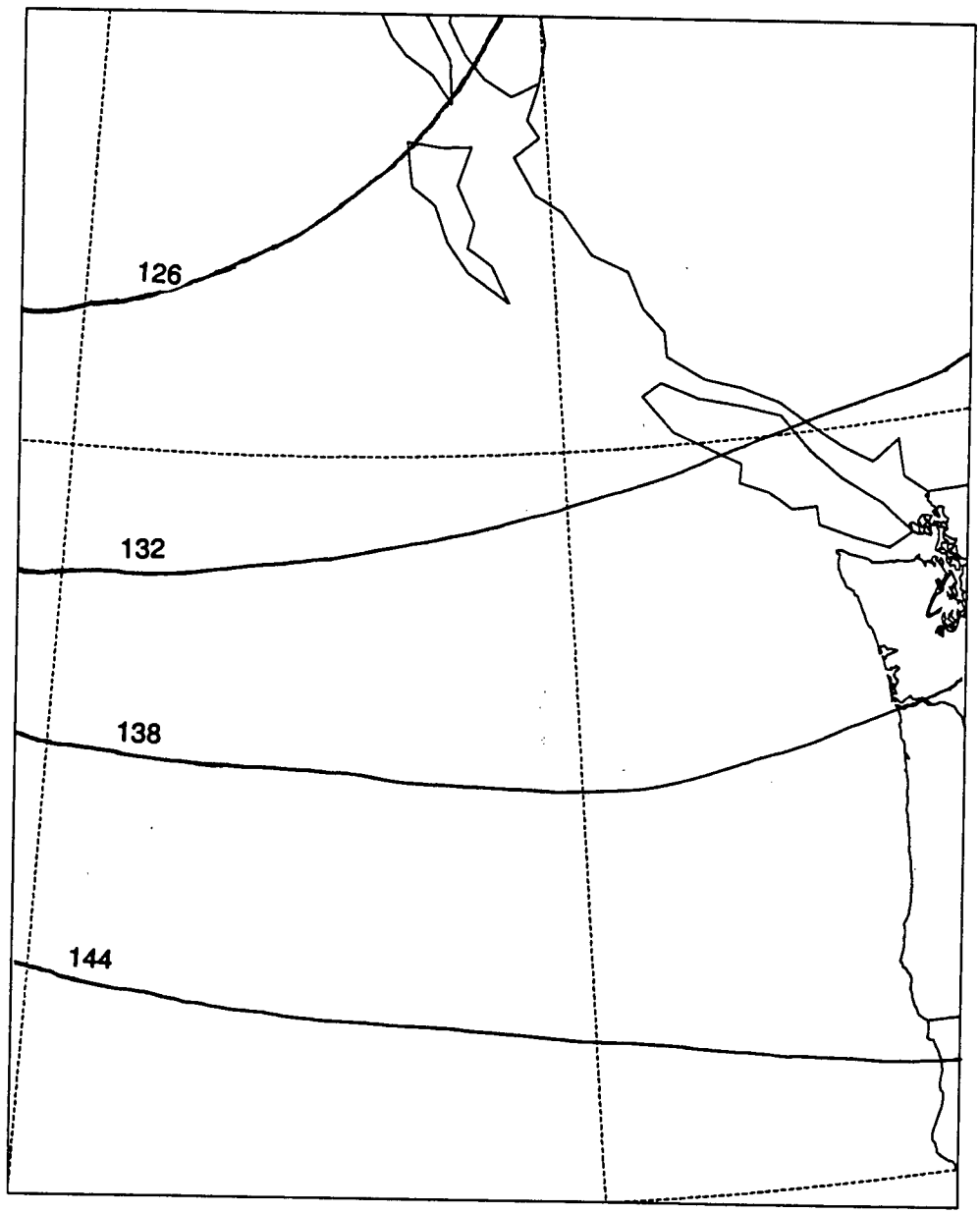

Figure 4.3: 24 November 1989 12:00Z, 850 mb geopotential height contours, in decameters

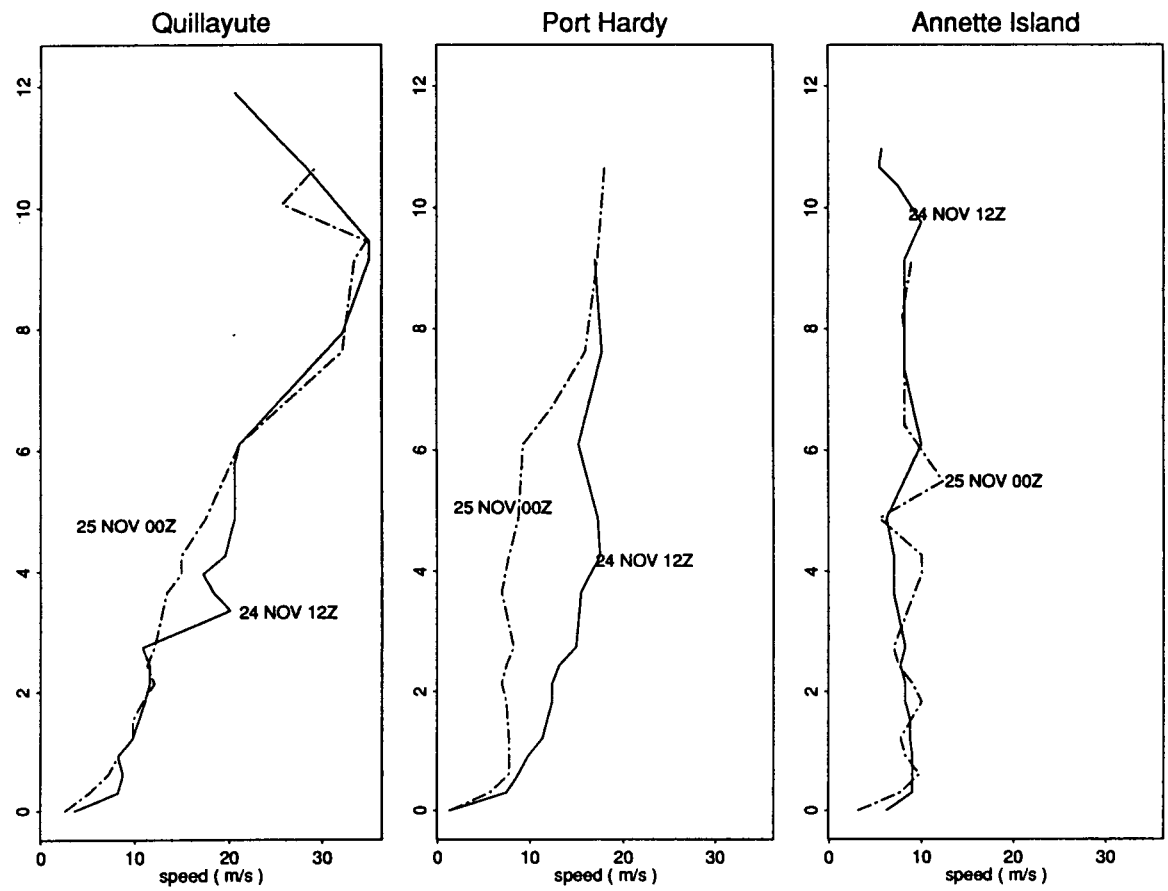

Figure 4.4: 24 November 1989, upper air wind reports for Annette Island, Port Hardy and Quillayute

Semi-automatic Cloud Motion Winds	Manual Cloud Motion Winds	Buoy Winds	Geostrophic Winds	Rawindsonde Winds
No. of clouds tracked 48	No. of clouds tracked 48	Buoys	Level = 850 mb	Stations
No. rejected 6	No. rejected 0	46036	Height= 1.5 km	ANN, UIL
Speed (ms^{-1}):	Speed (ms^{-1}):	46184	Speed : 20 to 25ms^{-1}	
Mean 16	Mean 17	46204		Distance from clouds:
Minimum 8	Minimum 9	46206		1000 to 1400 km
Maximum 23	Maximum 24	46207		
Std.Dev. 2.8	Std.Dev. 3.4	46208		Speed at 1.5 km:
		46208		5 to 8ms^{-1}
		Speed: 12ms^{-1}		Speed at 2.5 km:
				4 to 7ms^{-1}
Height of clouds: 2.5km	Height of clouds: 2.5km			
Time: 17:30 to 19:30Z	Time: 17:30 to 19:30Z	Time: 15 to 20Z	Time: 12Z	Time:16 Feb, 00Z
				16 Feb, 12Z

Table 4.2: Summary of Data Collected and Analyzed on 16 February, 1990

4.6 shows the surface analysis for 18:00Z. The surface wind moved cyclonically around a low pressure center located near ($57°N$, $143°W$).

Only one buoy, 46005, had collocated cloud motion vectors. The surface and cloud data are plotted in figure 4.7. The buoy speed was $8ms^{-1}$ at 17:00Z, $7ms^{-1}$ at 18:00Z and $9ms^{-1}$ at 19:00Z. The speed of the cloud motion vectors varied from 9 to $17ms^{-1}$ with an mean of $13ms^{-1}$. Except for 19:00Z, when the buoy observation was measured 1.5 hours after the cloud motion observations, there was almost no directional shear between the surface and the cloud level data. The buoy direction shifted from 270°, to 260°, and then to 290° from 17:00Z to 19:00Z. The direction of the cloud motion vectors ranged from 265° to 273° with an mean of 267°.

4.0.2 Case Study - 16 February 1990

A summary of this day's data is given in table 4.2.

As seen in figure 2.3, an offshore flow of colder continental air, along with moderate winds resulted in the formation of cloud streets, which subsequently evolved into open hexagonal cells. On this day, 48 open hexagonal cells were tracked : 11 from 17:30Z to 18:00Z; 16 from 18:00Z to 18:30Z; 16 from 18:30Z to 19:00Z; and 12 from 19:00Z to 19:30Z. Of the 48 vectors, 6 were rejected using the criteria outlined in section 2.1.4. The remaining 42 vectors are charted on figure 4.8. Speeds ranged from 8 to $23ms^{-1}$, and

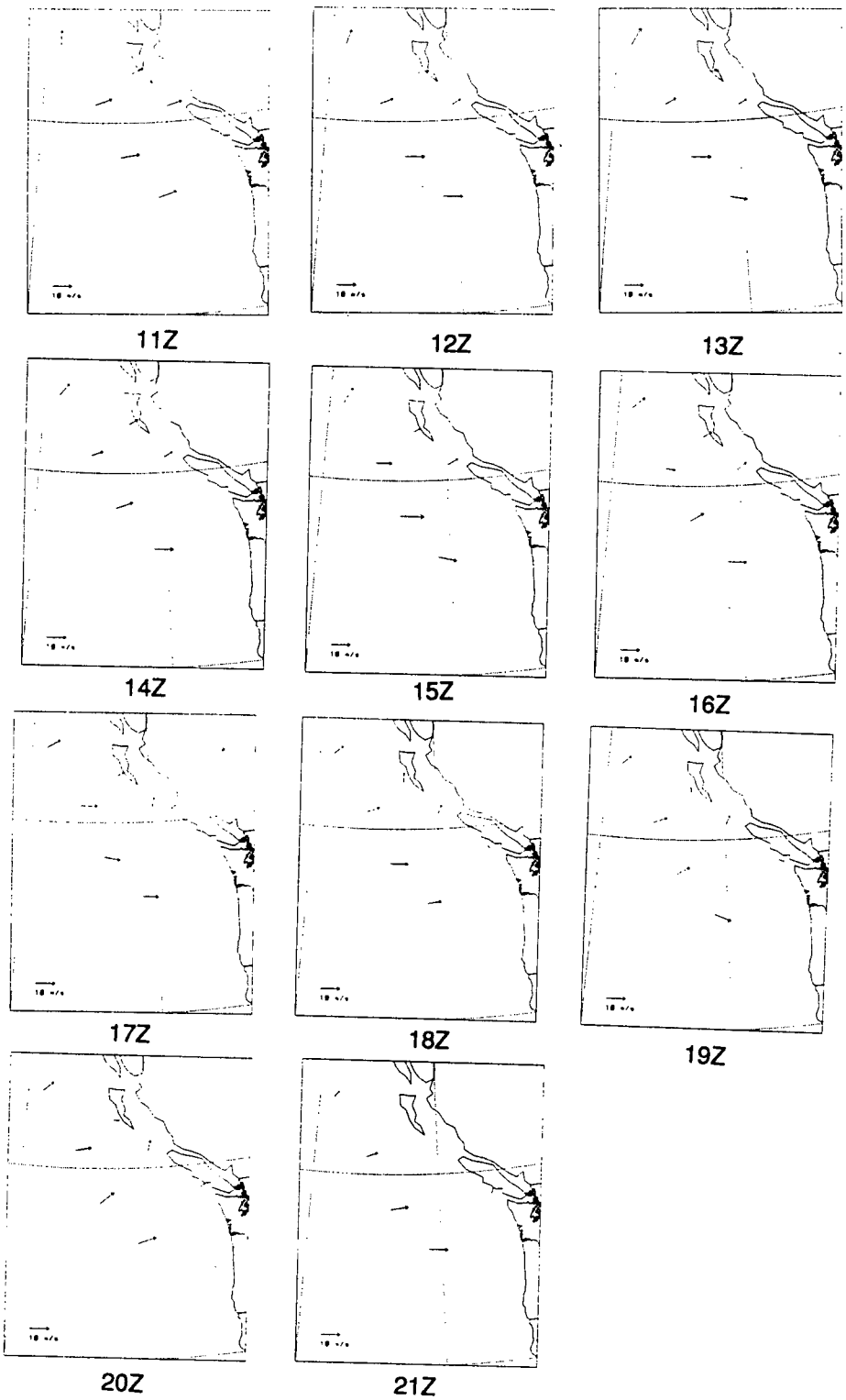

Figure 4.5: 24 November 1989, buoy winds collected from 11:00Z to 21:00Z

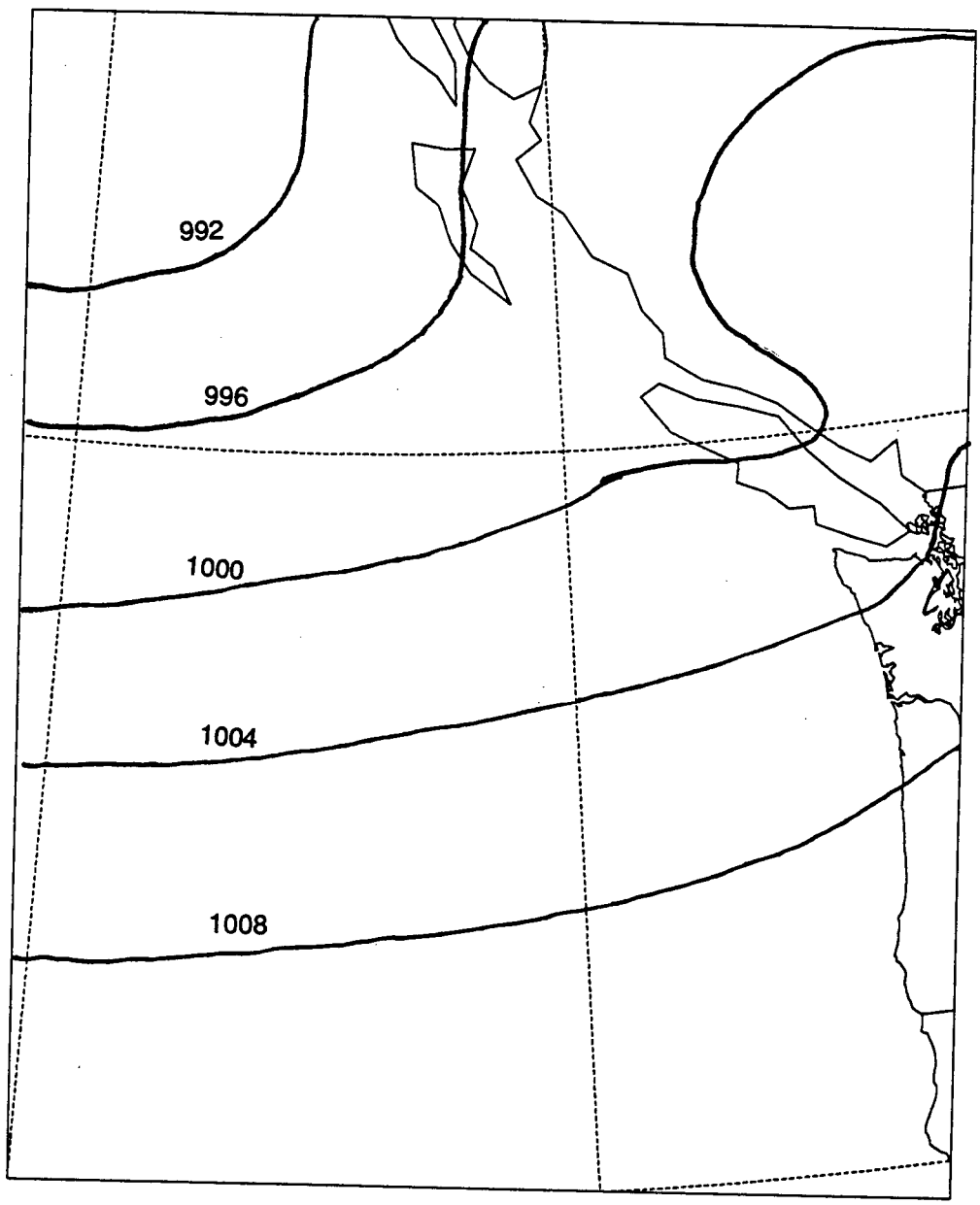

Figure 4.6: 24 November 1989, 18:00Z, surface analysis. Pressure contours in millibars

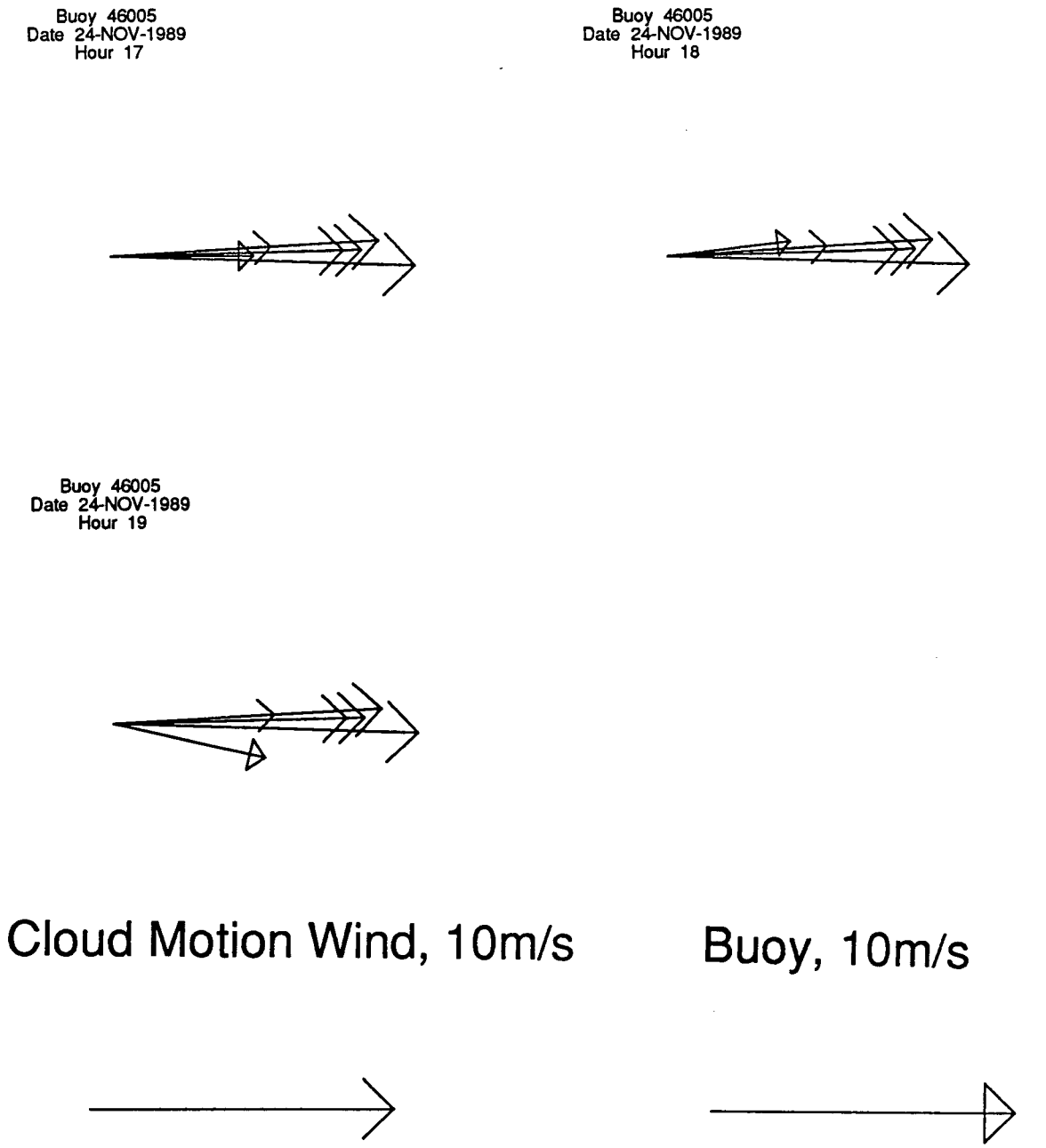

Figure 4.7: Collocated buoy wind and cloud motion vectors for 24 November 1989.

averaged 16ms^{-1} with a standard deviation of 2.8ms^{-1}. The wind direction shifted from north-northwesterly, at about 343°, in the north to northwesterly, at about 320°, in the south.

The same cloud targets were tracked manually (see figure 4.9). The mean speed of the manually tracked clouds was 17ms^{-1} with a minimum of 9ms^{-1} and a maximum of 24ms^{-1}. The directions of these vectors were from 19° to 354°, with vectors to the north being northerly, and to the south being northwesterly. Subjectively, the SSDA and manual vector sets are comparable.

Figure 4.10 shows the 850*mb* geopotential height contours generated by objective analysis for 16 February, at 12:00Z. Using the geostrophic wind approximation, the winds at 850mb, at approximately 1.5km above the ground, were estimated to be 20 ± 2ms^{-1} to 25 ± 4ms^{-1} in the region that the clouds were tracked.

Figure 4.11 shows the upper air radiosondes collected at 3 shore stations for 16 February, at 00:00Z and 12:00Z. Although Quillayute and Port Hardy are closer to the collected cloud motion vectors, wind measurements at Annette Island were probably more representative because of the synoptic pattern; there was a low pressure center situated between the region where the vectors were collected and Quillayute and Port Hardy. The Annette Island station is 1000 to 1400km from the vectors. At 1.5km, winds speeds at Annette Island were 5ms^{-1} at 00:00Z and 8ms^{-1} at 12:00Z.

Surface winds collected from 15:00Z to 20:00Z for 6 buoys (46036, 46184, 46204, 46206, 46207, 46208) are charted on figure 4.12, and the surface analysis for 18:00Z is charted on figure 4.13. The flow on both charts matched that observed tracking the clouds, moving cyclonically around a low pressure center, located at (46°N, 124°W). At the top of the ridge, the winds were northeasterly. Farther south, they became northerly, and then northwesterly.

Only one buoy, 46036, had collocated cloud motion vectors. The surface and cloud

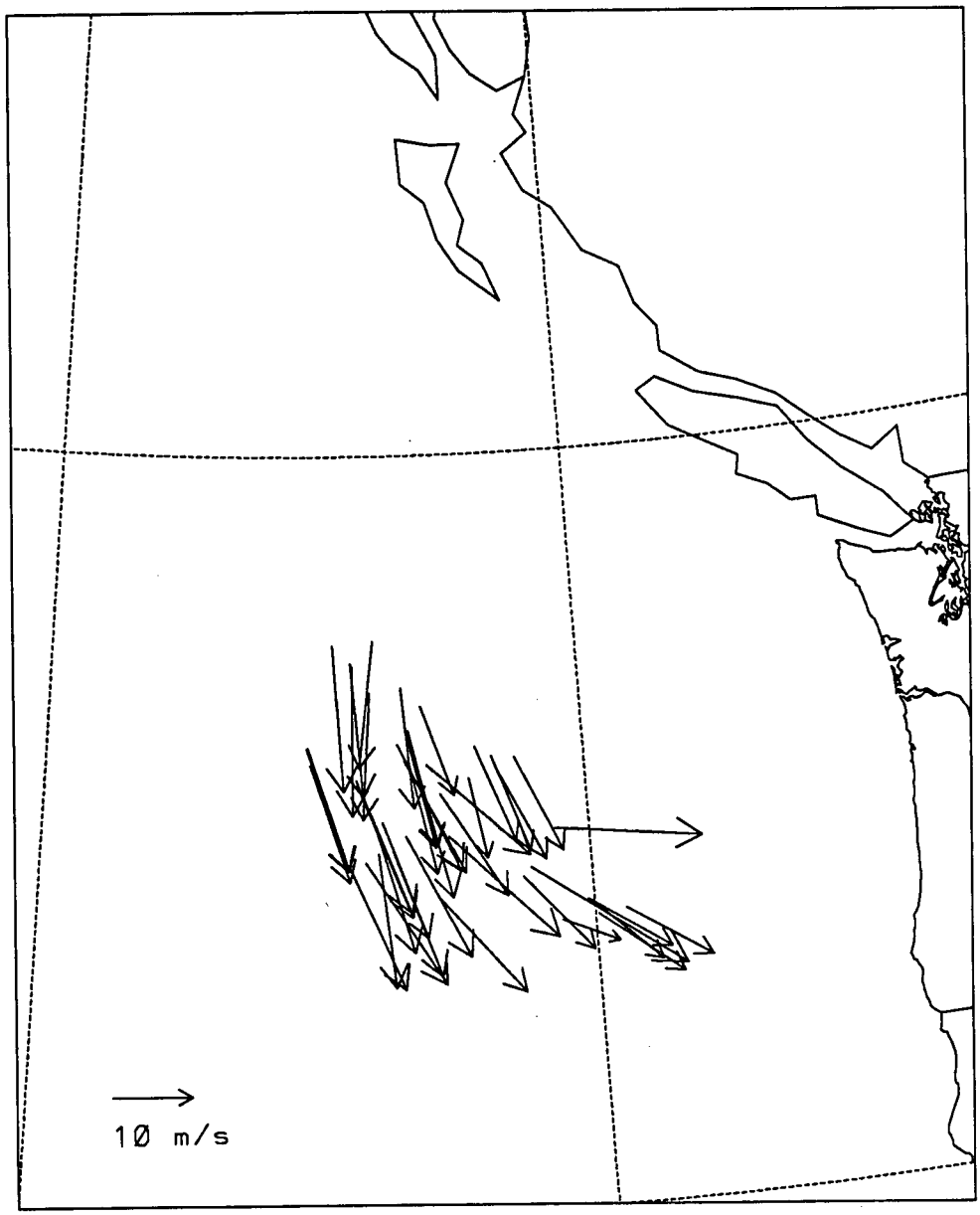

Figure 4.8: 16 February 1990, SSDA tracked cloud motion vectors collected from 17:30Z to 19:30Z

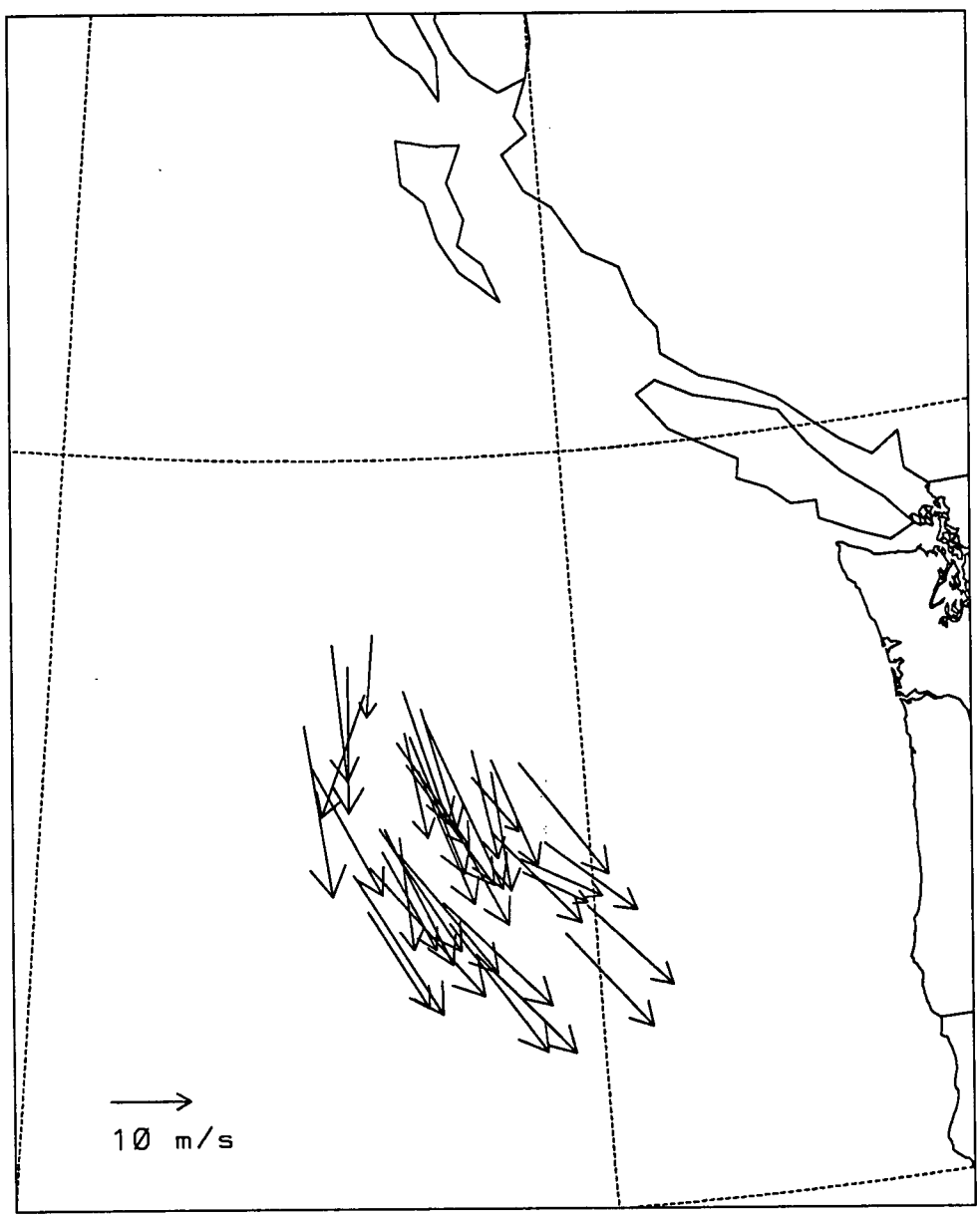

Figure 4.9: 16 February 1990, manually tracked cloud motion vectors collected from 17:30Z to 19:30Z

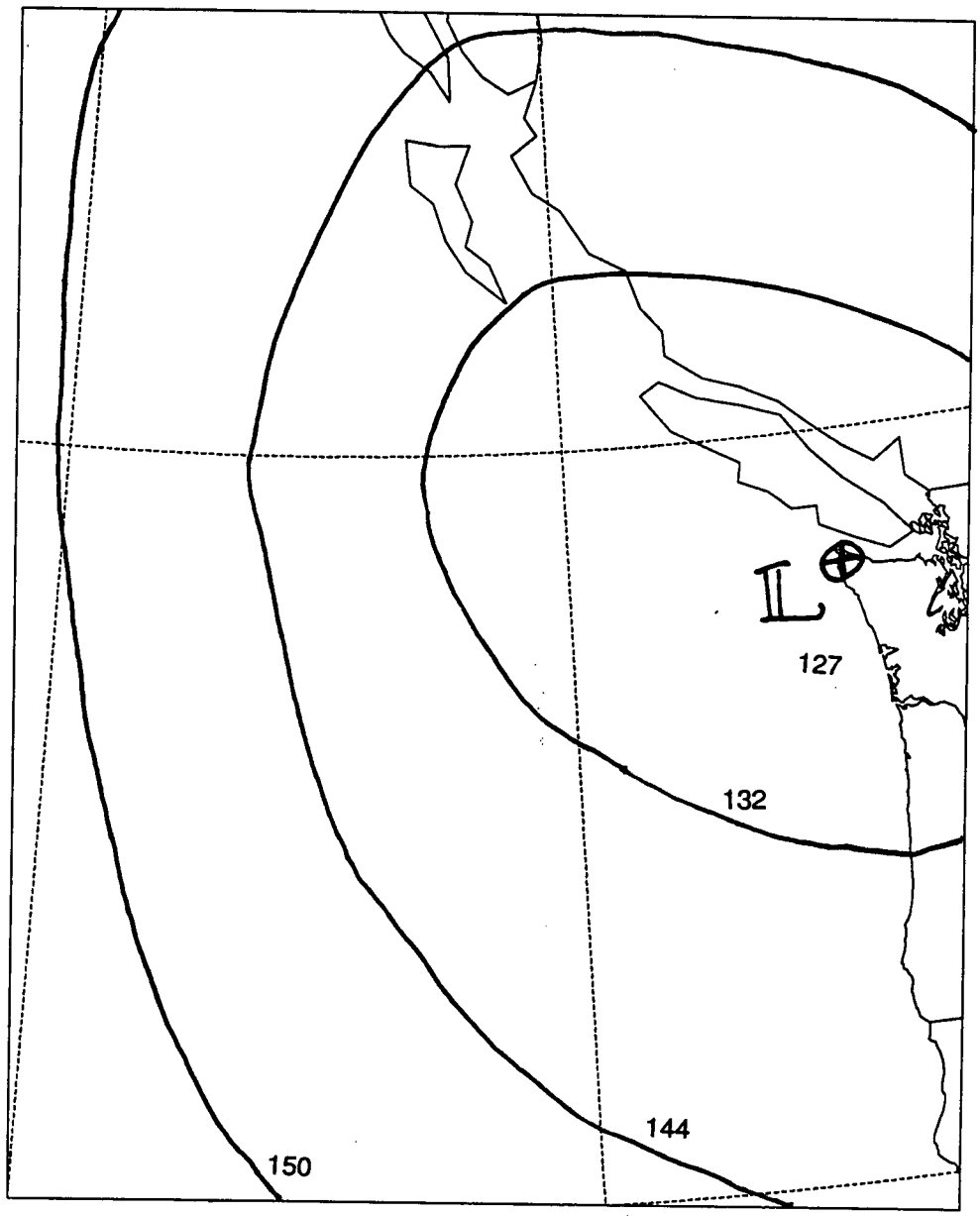

Figure 4.10: 16 February 1990 12:00Z, 850 mb geopotential height contours, in decameters

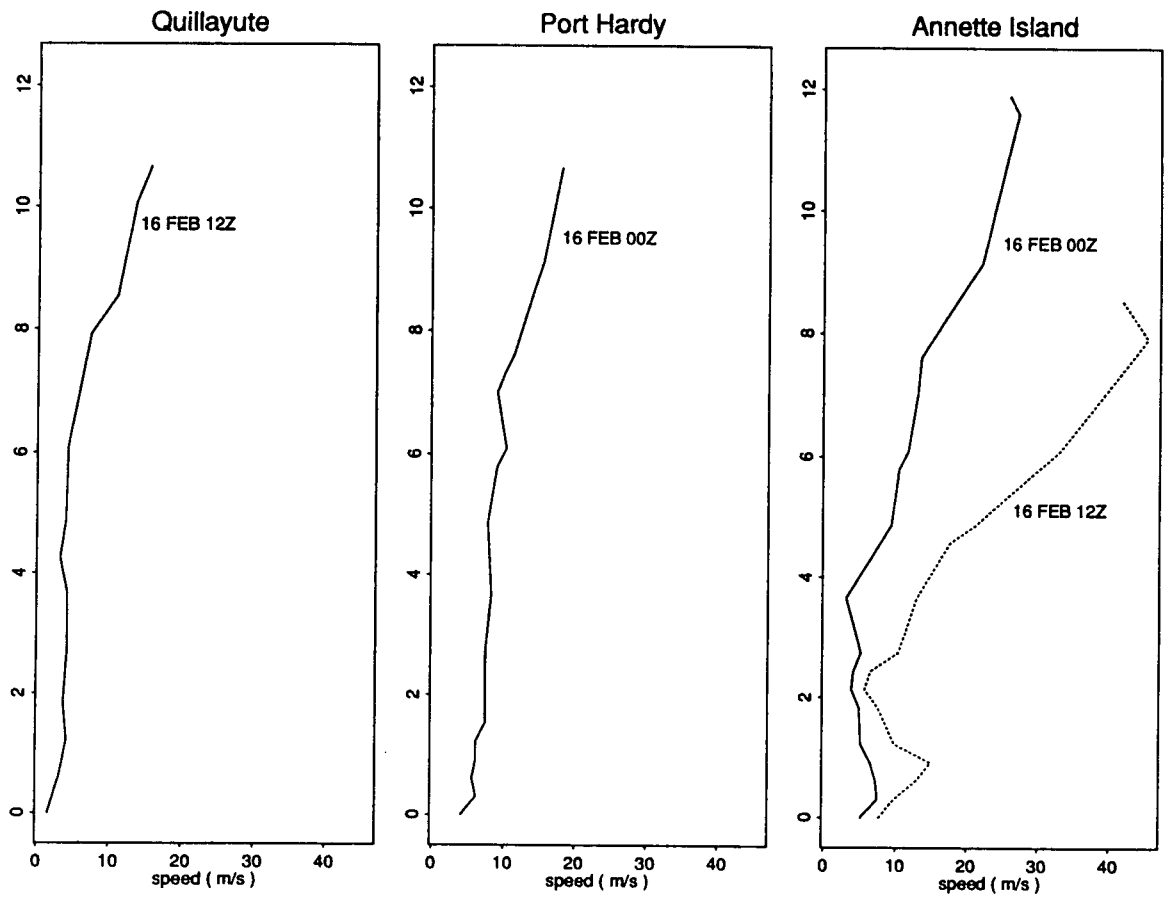

Figure 4.11: 16 February 1990, upper air wind reports for Annette Island, Port Hardy and Quillayute

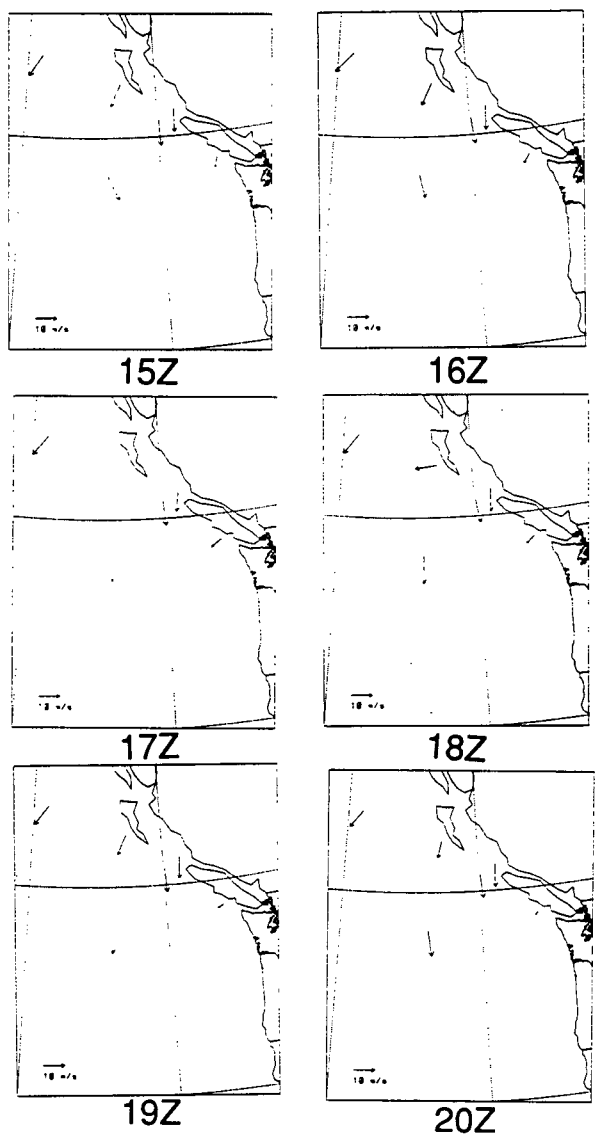

Figure 4.12: 16 February 1990, buoy winds collected from 15:00Z to 20:00Z

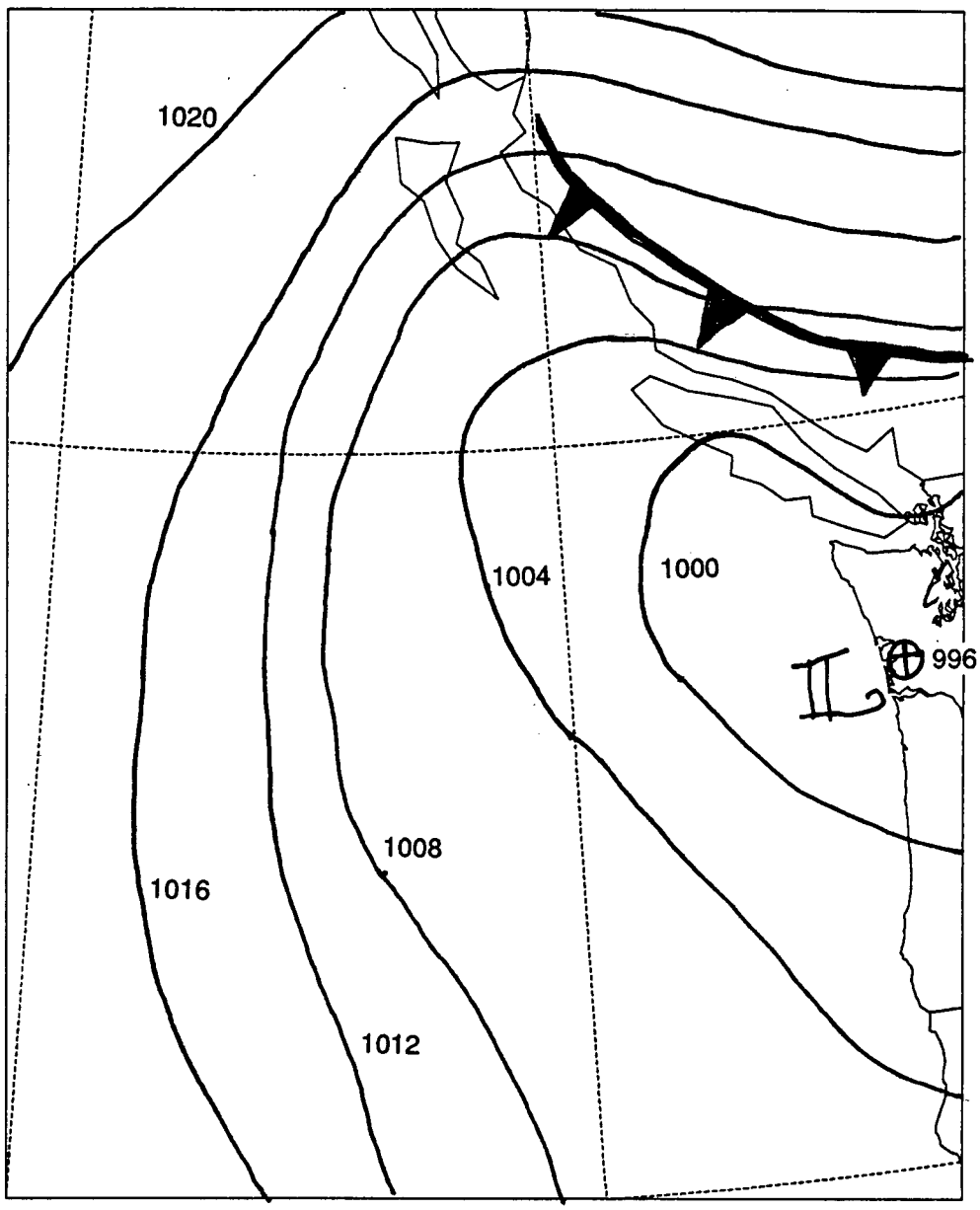

Figure 4.13: 16 February 1990, 18:00Z, surface analysis. Pressure contours in millibars

Semi-automatic Cloud Motion Winds	Manual Cloud Motion Winds	Buoy Winds	Geostrophic Winds	Rawindsonde Winds
No. of clouds tracked 47	No. of clouds tracked 47	Buoys	Level = 850 mb	Stations
No. rejected 4	No. rejected 0	46002	Height= 1.5 km	ANN, UIL
Speed (ms^{-1}):	Speed (ms^{-1}):	46005	Speed : 24 to 39ms^{-1}	
Mean 23	Mean 21	46036		Distance from vectors:
Minimum 14	Minimum 13	46184		300 to 1000km
Maximum 28	Maximum 28	46204		
Std.Dev. 2.9	Std.Dev. 3.3	46207		
		46208		
Direction (^{o}):	Direction (^{o}):			
Mean 241	Mean 242	Mean speed:		
Minimum 221	Minimum 209	$12ms^{-1}$		
Maximum 256	Maximum 255	Direction:		
Std.Dev. 7.6	Std.Dev. 5.1	165^o in north		Time: 5 Jan, 00Z
		230^o in south		5 Jan, 12Z
Time: 19:30 to 21:00Z	Time 19:30 to 21:00Z	Time: 16 to 21Z	Time: 12Z	6 Jan, 00Z

Table 4.3: Summary of Data Collected and Analyzed on 5 January, 1990

data is plotted in figure 4.14. Buoy speeds for the period averaged $12ms^{-1}$. Cloud motion vector speeds were from 17 to $19ms^{-1}$. As with the November day, there is a very weak directional shear, with the mean buoy direction being northerly at 360°, while directions of the clouds varied from 355° to 5°.

4.0.3 Case Study - 5 January 1990

As well as collecting cloud motion vectors the two days that open hexagonal cells, vectors were collected from disorganized cumulus clouds on 5 January 1990. Table 4.3 gives a summary of the data collected on this day.

On this day, seen on figure 2.2, unorganized cumulus developed behind an advancing cold front. There were 47 clouds tracked : 19 from 19:30Z to 20:00Z; 14 from 20:00Z to 20:30Z; and 14 from 20:30Z to 21:00Z. Of the 47 vectors, 4 were rejected using the criteria outlined in section 2.1.4. Of the remaining vectors, speeds ranged from 14 to $28ms^{-1}$ with an mean speed was $23ms^{-1}$ and a standard deviation of $2.9ms^{-1}$. Vector directions were southwesterly, ranging from 221 to 256° with an mean of 241° and a standard deviation of 7.6°.

The 47 clouds were also tracked manually, with the resulting vectors shown on figure 4.16. There is a close agreement between the results of the two methods. Speeds

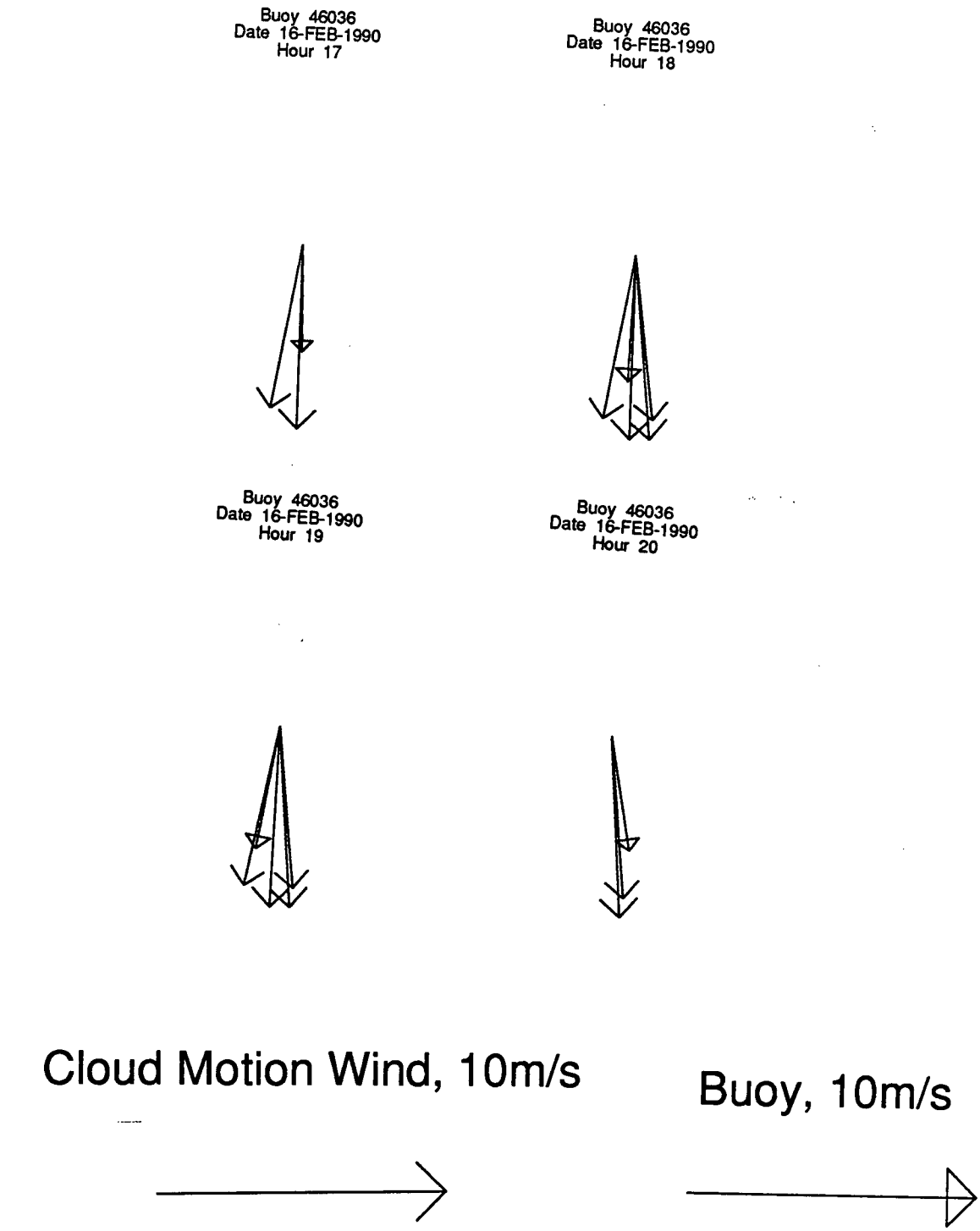

Figure 4.14: Collocated buoy wind and cloud motion vectors for 16 February 1990.

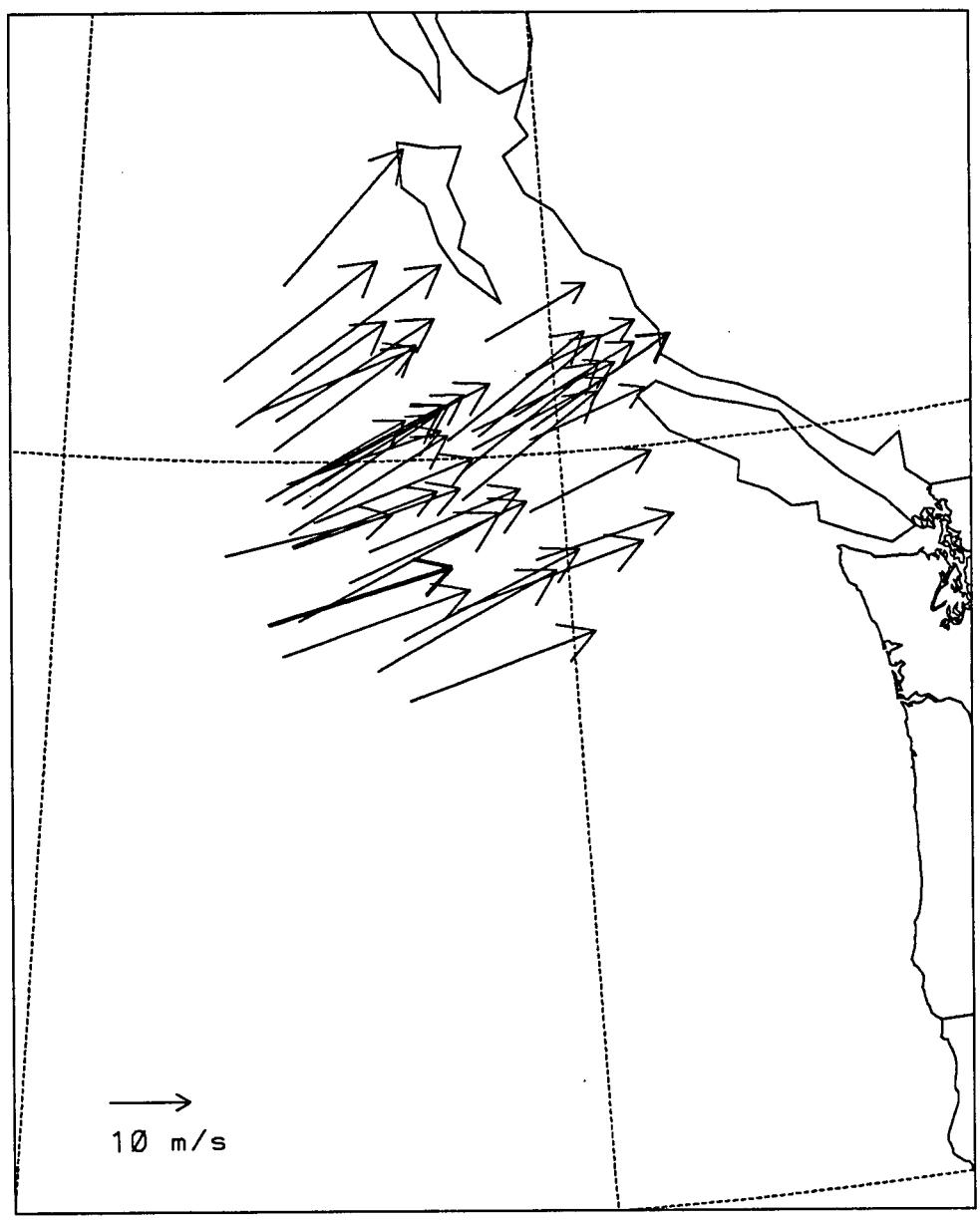

Figure 4.15: 5 January 1990, SSDA tracked cloud motion vectors collected from 19:30Z to 21:00Z

ranged from 13ms^{-1} to 28ms^{-1}, with an mean speed of 21ms^{-1} and standard deviation of 3.3ms^{-1}. The direction varied from 209° to 255° and averaged 242° and a standard deviation of 5.1°.

Figure 4.17 shows the 850mb geopotential height contours generated by objective analysis for 5 January, at 12:00Z. Using the geostrophic wind approximation, the winds at 850mb, at approximately 1.5km above the ground, were estimated to be between 24 $\pm$ 2ms^{-1} and 39 $\pm$ 7ms^{-1} in the region that the clouds were tracked.

Figure 4.18 shows the upper air radiosondes collected at 3 shore stations for 5 January, at 00:00Z and 12:00Z, and 6 January at 00:00Z. Annette Island and Port Hardy are downstream of the region where the vectors were collected. Winds at 1.5km, the level of the 850mb pressure level, increased from 9 to 28ms^{-1} at Port Hardy from 00:00Z to 12:00Z. At Annette Island, winds increased from 5 to 15ms^{-1} over the 24 hour period.

Surface winds were collected from 16:00Z to 21:00Z for 8 buoys (46002, 46004, 46005, 46036, 46184, 46204, 46207, 46208). Figure 4.19 charts the buoy winds for this time period. At 46184, the northerly most buoy, speeds ranged from 11 to 13ms^{-1}, with a southeasterly direction of 160° to 170°. Farther to the south, at buoy 46036, the flow was southwesterly, with winds from 220° to 240m°, and speeds of 12 to 15ms^{-1}. Away from the land, the mean wind speed was 12ms^{-1} with a standard deviation of 2.0ms^{-1}. There was far less coherence in the near shore buoys (46204, 46207, 46208), where topography disrupted the uniform wind pattern observed farther offshore. Figure 4.20 shows the the surface analysis for 18:00Z. Moderate and steady surface winds moved cyclonically around a low pressure center located at (55°N, 145°W).

Figure 4.21 compares the buoy winds with their collocated cloud motion winds for four buoys. In all but one case, winds were turning clockwise (veering) with height. The largest directional difference occurs for the near-shore buoy, 46207. At this point, and

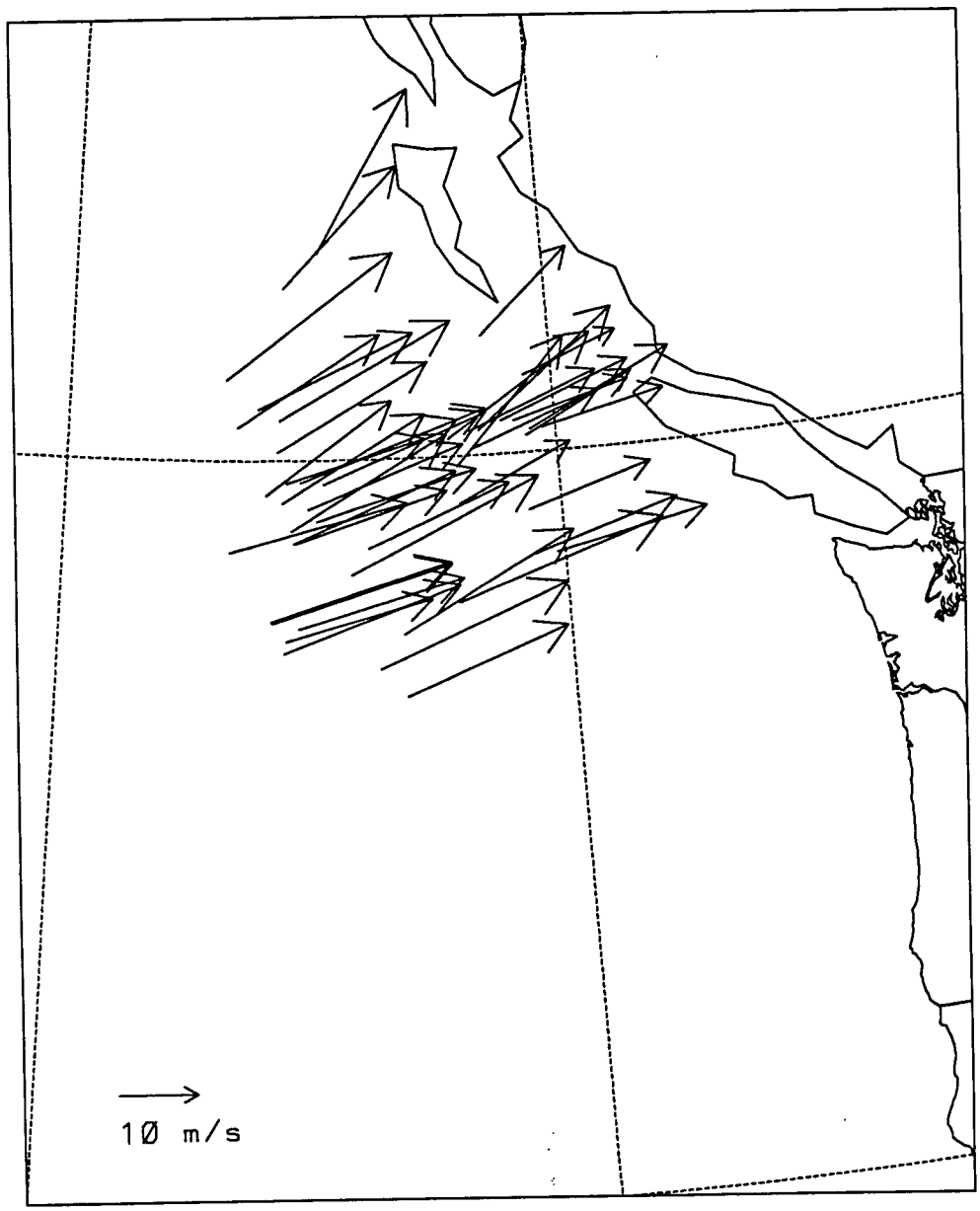

Figure 4.16: 5 January 1990, manually tracked cloud motion vectors collected from 19:30Z to 21:00Z

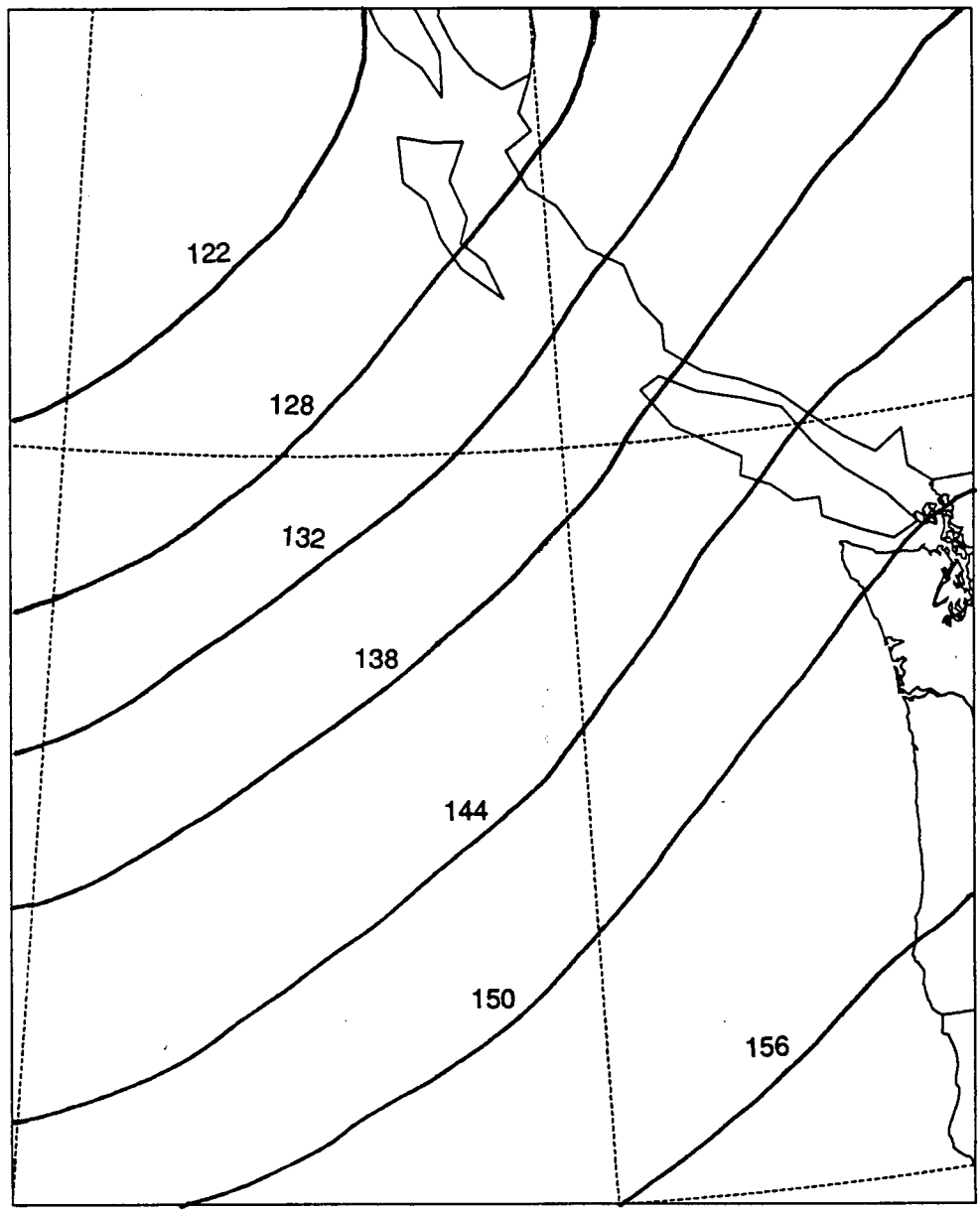

Figure 4.17: 5 January 1990 12:00Z, 850 mb geopotential height contours, in decameters

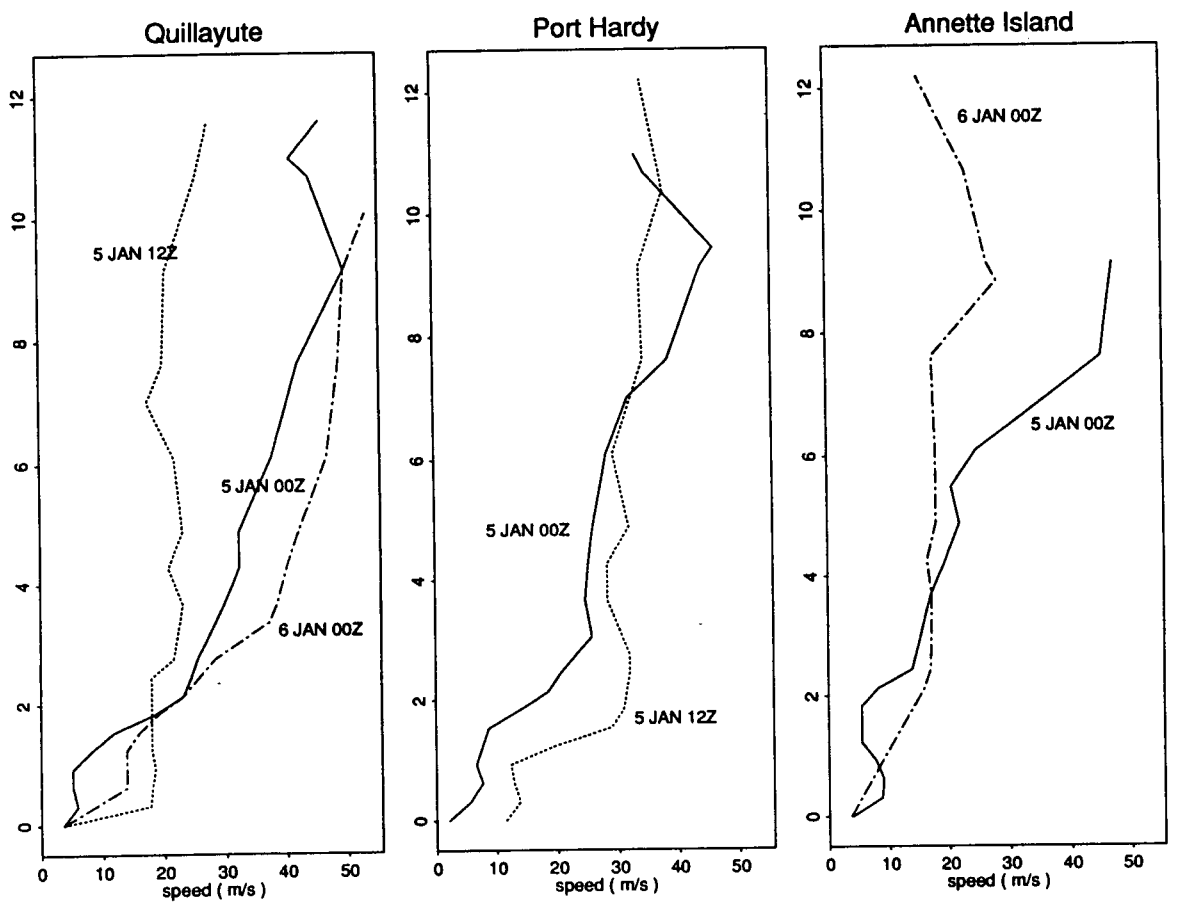

Figure 4.18: 5 January 1990, upper air wind reports for Annette Island, Port Hardy and Quillayute

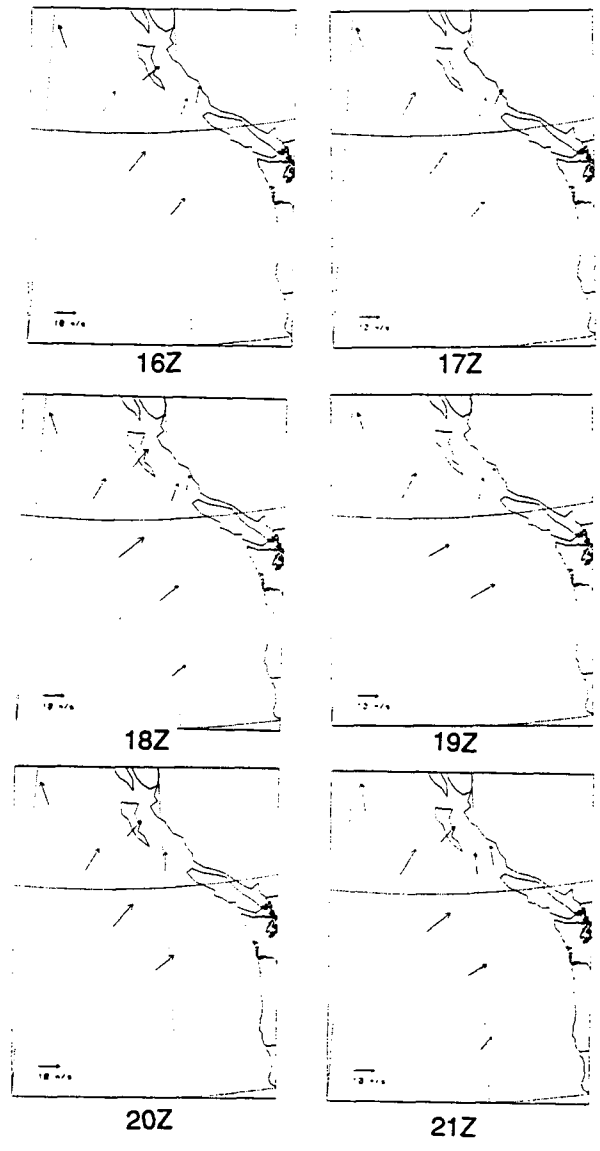

Figure 4.19: 5 January 1990, buoy winds collected from 16:00Z to 21:00Z

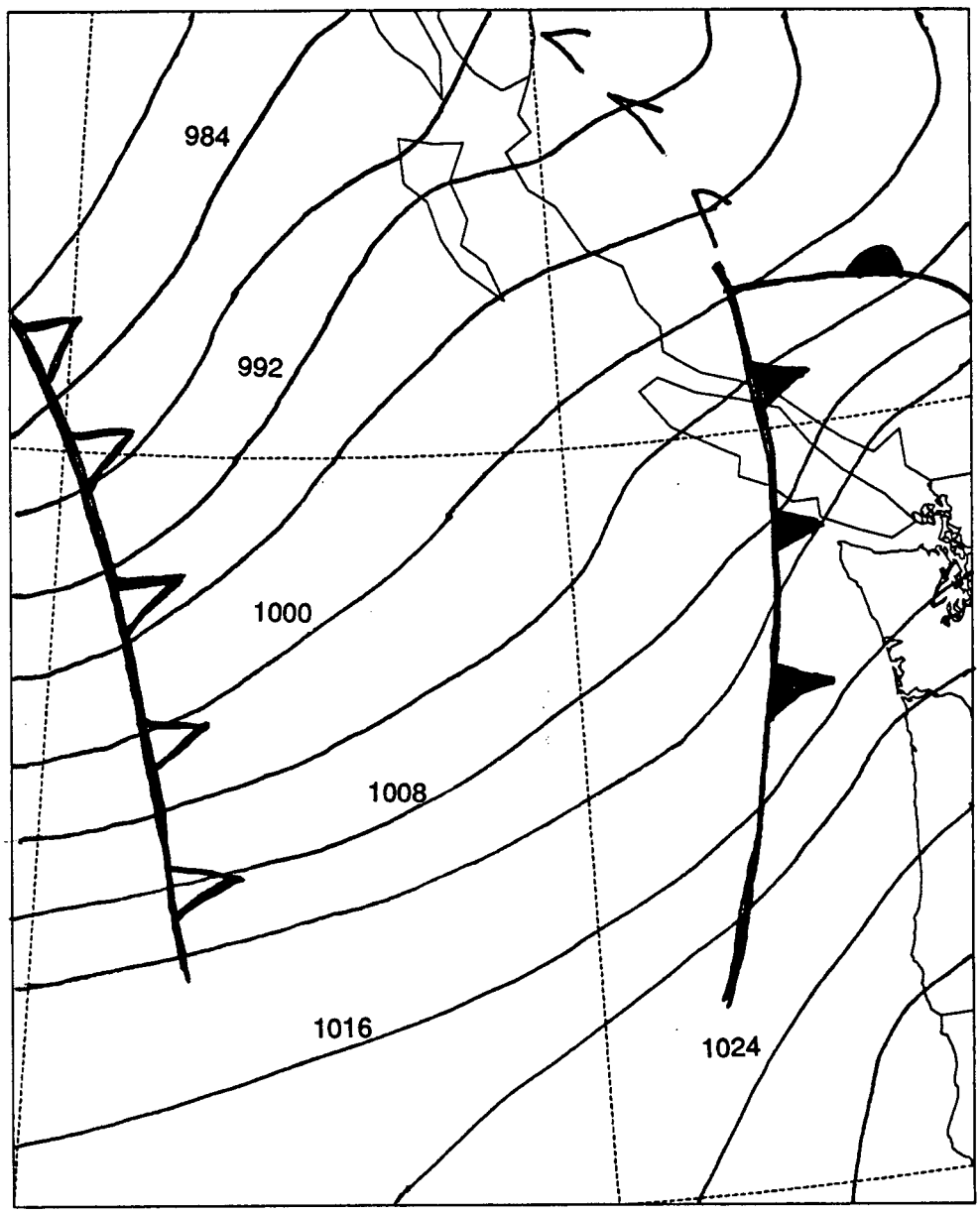

Figure 4.20: 5 January 1990, 18:00Z, surface analysis. Pressure contours in millibars

also for buoy 46208, topography may be influencing the surface wind. For the two offshore buoys, the mean speed was 13ms^{-1}. Cloud motion vectors were from 20 to 29ms^{-1}, and mean 23ms^{-1} at 46004, and 25ms^{-1} for 46036. The mean directional shear was 27° for 46004, and 14° for 46036.

4.1 Discussion

Overall, for all three days, there was consistency between the cloud motion vector directions and the synoptic pattern at the surface and other upper level wind measures. There was also a strong agreement between the SSDA tracked clouds and the manually tracked clouds. There is not as much consistency between cloud tracked winds and other measures of upper level wind speeds. However, the rawindsonde data is far removed from the region the clouds were tracked. The geopotential height analysis is generated from upper air rawindsonde data which is extremely sparse over the oceans, making wind wind estimates from these charts questionable.

The objectives of this study was to compare cloud motion vectors of open hexagonal cells with buoy wind reports. In the end, there was little ground truth (1 buoy on 24 November 1989, 1 buoy on 16 February 1990) to compare the cloud motion winds with. This is not surprising since there was a limited set of images to analyze, and because the buoys are widely scattered.

There was also agreement between the directional shears between the collocated buoy and cloud motion winds and other observations and theories. Except for cloud motion data collocated with buoy 46005 on 24 November at 19:00Z, there was almost no directional shears for the open hexagonal cell vectors. Agee and Dowell (1974) found that the mean directional shear between the surface and winds at the top of the boundary layer for open hexagonal cells was $-6°$. One of the requirements for open hexagonal cells

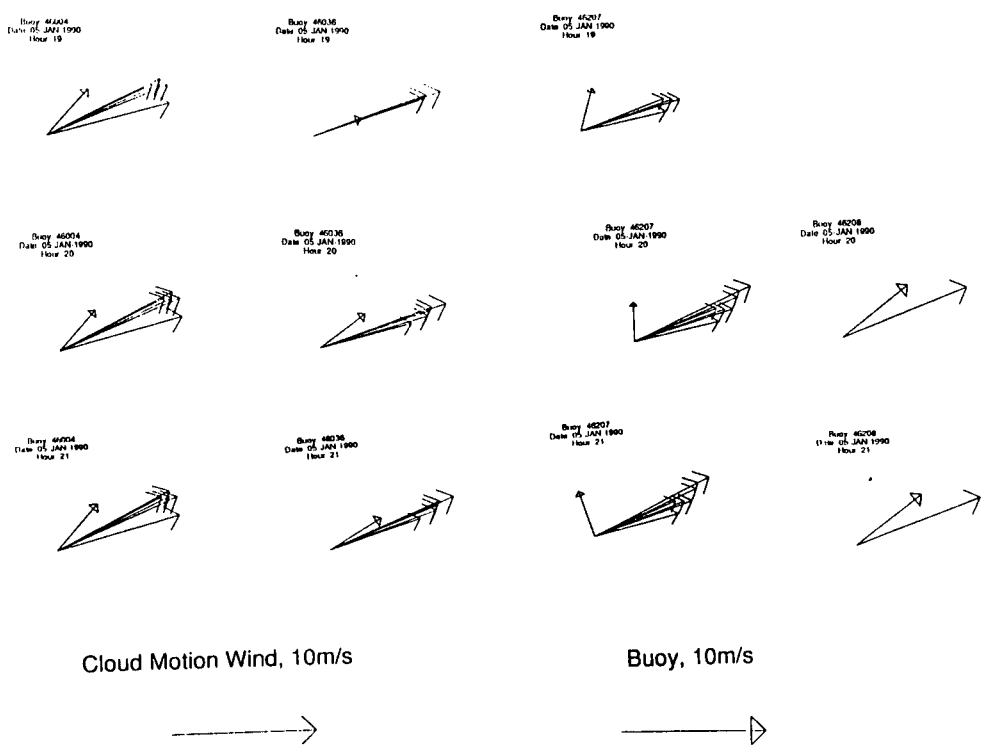

Figure 4.21: Collocated buoy wind and cloud motion vectors for 5 January 1990.

to form is a small shear between the surface and the top of the boundary layer. Strong shears create turbulence which destroys the uniform circulation patterns. The shear in the layer is also reduced by the roll structure of the cells mixing momentum throughout the layer. On the other hand, the January day with unorganized cumulus cloud, which had shears of 14° to 27°, is more like an ideal Ekman boundary layer in which surface friction, pressure gradient, and Coriolis force determine the wind field in the absence of convective mixing of momentum. For the January day, the air-sea temperature difference, which averaged 0°C at the buoy locations, is indicative of a stable boundary layer, where there is an absence of convective activity. In contrast, the negative air-sea temperature differences on the November and February days, averaging −4°C and −5°C at the buoys, generated an unstable boundary layer with convective mixing.

In a stable boundary layer, the horizontal equations of motion are approximately (Holton, 1979):

$$-fv = -\frac{1}{\rho}\frac{\partial p}{\partial x} + \frac{\partial \tau_x}{\partial \rho} \tag{4.11}$$

$$fu = -\frac{1}{\rho}\frac{\partial p}{\partial y} + \frac{\partial \tau_y}{\partial \rho} \tag{4.12}$$

where f is the Coriolis parameter, $U = (u, v)$ is velocity, ρ is density, $\frac{\partial p}{\partial x}$ and $\frac{\partial p}{\partial y}$ are the horizontal pressure gradients, $\frac{\partial \tau_x}{\partial \rho}$ and $\frac{\partial \tau_y}{\partial \rho}$ are the horizontal eddy stress gradients caused by the surface friction. The Ekman boundary layer model is a matched solution to this approximation.

At the ground, the velocity is zero. In the few meters above the ground, called the surface layer, surface stress is approximately constant. The solution of 4.11, and 4.12 is approximately

$$u = \frac{u_*}{k}\ln(\frac{z}{z_o}) \tag{4.13}$$

where $u_* \simeq 0.3\text{ms}^{-1}$ is the friction velocity, $k \simeq 0.4$ is von Karman's constant, z is the height within the layer, and z_o is the roughness length, which is about 10^{-3}cm over water (Brown and Liu,1984). Here, the flow near the ground is parallel to the y-axis.

At the top of the layer, we assume the wind field is geostrophic, so that

$$-fv = -\frac{1}{\rho}\frac{\partial p}{\partial x} = -fv_g \tag{4.14}$$

$$fu \equiv -\frac{1}{\rho}\frac{\partial p}{\partial y} = fu_g \tag{4.15}$$

where $V_g = (u_g, v_g)$ is the geostrophic wind.

To find the wind $U = (u, v)$ at level z within the layer, 4.13 is matched with 4.14 and 4.15 yields the solution

$$u = u_g(1 - e^{-\gamma}\cos\gamma z) \tag{4.16}$$

$$v = u_g e^{-\gamma}\sin\gamma z \tag{4.17}$$

where $\gamma = (f/2K)^{1/2}$, $K \simeq 5\text{m}^2\text{s}^{-2}$ is the eddy viscosity. Figure 4.22, calculated for representative values of z_o, u_*, and K, shows how wind increases and veers with height. There is a directional shear of 15^o between the wind at 3m above the surface and at the top of the boundary layer.

While the vectors were consistent with the direction of the flow, there was far more variation in wind speed than would be expected if the vectors all measured cloud motions of open hexagonal cells at the same level. Agee and Dowell's (1974) observations of 25 cases of open hexagonal cells are a guide to the variation in wind speeds expected. The standard deviations for the November, and February days, 3.4ms^{-1}, and 2.9ms^{-1} respectively, are greater than their observed $2.25\text{ms}^{-1}\text{km}^{-1}$ mean vertical shear over 1 kilometer. If the vertical shear on the November and February days was 2.25ms^{-1} and

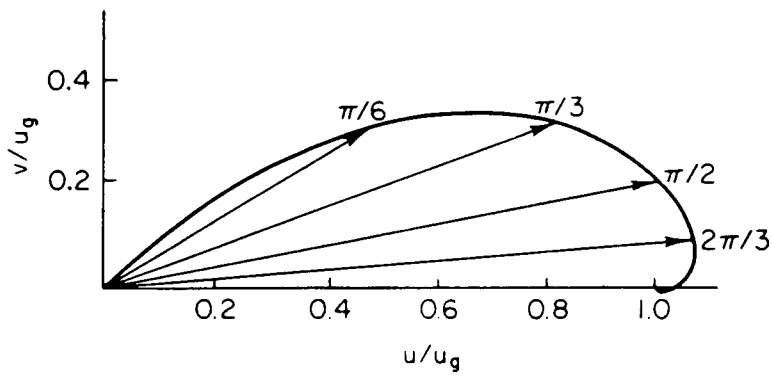

Figure 4.22: Vertical wind profile of the Ekman boundary layer wind field. Points on curve are values of γz, which is a nondimensional measure of height (from Holton, 1979).

the collected vectors represented speeds of winds in the atmosphere at various levels, then the difference between the maximum and minimum speeds for the two days of $11ms^{-1}$ and $15ms^{-1}$ represents a difference in heights of 4.8 and 6.7km.

The large variation in the speeds could be caused because the vectors were measuring speeds at various heights, or because the tracking algorithm is not satisfactory. The latter seems the more likely explanation. When the motion of the clouds were examined subjectively, there is no observed divergence or convergence within the motion of the open hexagonal cells. The cells in the tracking region move at a uniform speed. Since there was as wide of variation in speed for manually tracked clouds, the variation may be caused by systematic errors, rather than the SSDA tracking algorithm.

Chapter 5

Discussion and Conclusions

This study investigated a number of problems dealing with cloud motion winds of open hexagonal cells. The three parts of the study mirrored the three steps taken by forecasters at the Pacific Weather Centre (PWC) when using cloud motion winds for surface marine forecasts: the collection of cloud motion vectors; the assignment of a vector to a specific height; and the estimation of a surface wind field from the motion of the clouds aloft.

The collection of the cloud motion vectors was done using a algorithm fashioned after Barnea and Silverman's (1972) Sequential Similarity Detection Algorithm (SSDA). This particular algorithm was chosen because it was easy to implement and because of its operational success at NASA Marshall Space Flight Center. The wind estimates from the SSDA method were comparable to wind estimates from manual tracked clouds. When compared with two other measures of winds - geostrophic winds from geopotential height analysis, and upper wind rawindsonde observations - there was less consistency. However, the geopotential height analysis is generated from upper air rawindsonde observations, which are sparse over the oceans, and the rawindsonde observations were spatially and temporally distant from the cloud motion vector data.

The nature of the open hexagonal cells, with their homogeneous flat tops and well understood vertical shear characteristics, lends itself to studying the problem of height assignment of cloud motion vectors. Two approaches that are often used for finding the temperature of the cloud top - minimum temperature and threshold - were both shown to be unsuitable. The minimum temperature was not the same for all of the

clouds that were tracked. The threshold method was arbitrary and could not be relied on to give the minimum temperature of open hexagonal cells. Since these methods do not work for the open hexagonal cells, it seems unlikely that they would correctly estimate the height of the cloud tops for unorganized cumulus which have varying cloud top heights. Coakley/Bretherton diagrams proved useful in determining the sea surface temperature and detecting cirrus. On the February day, when cloud streets were present, this technique was able to find the cloud top height. For the November day, the cloud top temperature was found by using both the visible and infrared channels, and finding the coldest pixel that was located on a hexagonal cell wall.

The small data set does not allow for an empirical relationship between surface and cloud motion winds of open hexagonal cells to be formulated. However, the agreement of this small set of data with other observations on open hexagonal cells underscores to importance of differentiating cloud type when inferring surface winds from cloud motions aloft. In comparing 10 months worth of cloud motion vectors with buoy winds at one location, Halpern and Knox (1983) did not find a correlation between the two measurements on daily basis. Only when the data was averaged over 15 days was there a correlation. But their study did not differentiate between cloud types. In this study, for the two days with open hexagonal cells, where there was almost no directional shear, On the day with unorganized convection, shears from 14° to 27° between the buoy and the clouds were measured. Differences in speed and directional shears for different convective stability regimes, which generate different cloud types, have also been found in numerical model work by Brown and Liu (1982) and Brown and Levy (1986). Future work in estimating surface winds from cloud motion winds at the synoptic scale should include differentiating between various cloud types and their associated boundary layer wind fields.

Appendix A

Glossary

AVHRR advanced very high resolution radiometer.

CMW cloud motion wind.

GAC global area coverage data.

IR infrared.

McIDAS man-computer interactive data access system.

MDA MacDonald Dettwiler and Associates (Richmond, B.C.).

METDAS Meteorological Data Analysis System.

METEOSAT European Space Agency current operational geostationary meteorological satellite

MSFC Marshall Space Flight Center

NASA National Aeronautics and Space Administration (Washington, D.C.).

NESDIS National Environmental Satellite and Data Information Services (NOAA) (Washington, D.C.).

NESS National Environmental Satellite Service (now part of NESDIS).

NOAA National Oceanic and Atmospheric Administration.

PWC Pacific Weather Centre (Vancouver, B.C.).

RADIOSONDE instruments attached to a helium balloon that measure the vertical distribution of temperature, moisture, pressure, wind speed, and wind direction.

SEASAT-A NASA polar-orbiting research oceanographic satellite (1978).

TIROS-N current operational U.S. civilian polar-orbiting meteorological satellite.

TOVS TIROS operational vertical sounder.

Bibliography

[1] AGEE, E. M. and K. E. DOWELL (1974) Observational Studies of Mesoscale Cellular Convection, *Journal of Applied Meteorology*, 13, 46-53

[2] BARNEA, D. I. and H. F. SILVERMAN (1972) A class of algorithms for fast digital image registration. *IEEE Transactions*, C-21, 179-186

[3] BENGTSSON, L., M. KANAMITSU, P. KALLBERG, and S. UPPALA, (1982) FGGE 4-Dimensional Data Assimilation at ECMWF, *Bulletin of the American Meteorological Society*, 63, 29-43

[4] BROWN, R. A. and W. T. LIU (1984) An Operaational Large-Scale Marine Planetary Boundary Layer Model, *Journal of Applied Meteorology*, 21, 261-269

[5] BROWN, R. A. and G. LEVY (1986) Ocean surface Pressure Fields from Satellite-Sensed Winds, *Monthly Weather Review* , 114, 2197-2205

[6] BUSCH, N. E. (1973) On the mechanics of atmospheric turbulence. *Workshop on Micrometeorlogy*, American Meteorological Society, 1-66

[7] COAKLEY, J. A. and F. P. BRETHERTON (1982) Cloud cover from high-resolution scanner data: detecting and allowing for partially filled fields of view, *Journal of Geophysical Research*, 87(C7), 4917-4932

[8] ENDLICH, R. M. and D. E. WOLF (1981) Automatic cloud tracking applied to GOES and METEOSAT observations, *Journal of Applied Meteorology*, 20, 309-319

[9] ERIKSSON, A. (1986) Quality of Cloud Motion Information from METEOSAT Imagery in the Norwegian Area, *Conference on Polar Lows, 1986, Oslo, Norway, May 20-23. Proceedings*, Meteorological Institute and Oceanographic Co. of Norway, 133-139

[10] GILHOUSEN, D. B. (1987) A Field Evaluation of NDBC Moored Buoy Winds, *Journal of Atmospheric and Oceanic Technology*, 4, 94-104.

[11] HALPERN, D. and R. A. KNOX (1983) Coherence between low-level cloud motion vectors and surface wind measurements near $0^o, 152^o$ from April 1979 to February 1980. *Atmosphere-Ocean* 21, 82-93

[12] HAMADA, T. (1985) The relationship between cloud motion winds from GMS and ocean surface winds from ship report over western Pacific Ocean, *Journal of the Meteorological Society of Japan*, 63, 959-967

[13] HASLER, A. F., W. E. SHENK and W. C. SKILLMAN (1977) Wind estimates from cloud motions: results from I, II and III of an in situ aircraft verification experiment, *Journal of Applied Meteorology*, 16, 812-815

[14] HASLER, A. F., W. C. SKILLMAN, W. E. SHENK and J. STERANKA (1979) In situ aircraft verification of the quality of satellite cloud winds over oceanic regions, *Journal of Applied Meteorology*, 18, 1481-1489

[15] HOLTON, J. R. (1979) *An Introduction to Dynamic Meteorology* , Academic Press, 391 pp

[16] HUBERT, L. F. (1979) Wind Derivation from Geostationary Satellites, in *Quantitative Meteorological Data from Satellites*, World Meterological Organization Technical Note No. 166, edited by J. S. Winston, 33-59.

[17] HUBERT, L. F. and A. THOMASELL, Jr. (1979) *Error Characteristics of Satellite-Derived Winds. NOAA Technical Report NESS 79*, 35 pp

[18] HUBERT, L. F. and L. F. WHITNEY, Jr. (1971) Wind estimation from geostationary-satellite pictures, *Monthly Weather Review*, 99, 665-672

[19] ISAACS, R. G., R. N. HOFFMAN and L. D. KAPLAN (1986) Satellite remote sensing of meteorological parameters for global numerical weather prediction, Reviews of Geophysics, 24, 701-743

[20] KRISHNAMURTI, R., (1970) On the transition to turbulent convection, *Journal of Fluid Mechanics*, 42, 295-320

[21] KRISHNAMURTI, R., (1975a) On Cellular Cloud Patterns. Part 2: Laboratory Model, *Journal of the Atmospheric Sciences*, 32, 1353-1372

[22] KRISHNAMURTI, R., (1975b) On Cellular Cloud Patterns. Part 3: Applicability of the Mathematical and Laboratory Models, *Journal of the Atmospheric Sciences*, 32, 1373-1383

[23] McLAREN (1990) personal communications, Atmospheric Environment Service, Environment Canada.

[24] MENZEL, P. (1984) NOAA NESS internal memorandum

[25] SADLER, J. C. and B. J. KILONSKY (1985) Deriving surface winds from satellite observations of low-level cloud motions, Journal of Climate and Applied Meteorology, 24, 758-769

[26] TURNER, J.S. (1973) *Buoyancy effects in fluids*, Cambridge University Press, 368 pp.

[27] VAN DELDEN, A. (1987) *On Cumulus Cloud Patterns and the Theory of Shallow Convection*, Ph. D. Thesis, College van Dekanen, Utrecht, Nederlands, (unpublished document)

[28] WESTON, K. J. (1980) An observational study of convective cloud streets, *Tellus*, 32, 433-438

[29] WHITNEY, L. F. (1983) International comparison of satellite winds - an update, *Advances in Space Research*, 2, 73-77

[30] WILSON, G, S. (1984) Automated Mesoscale Wind Fields Derived From GOES Satellite Imagery, *Preprints: Conference on Satellite Meteorology / Remote Sensing and Applications, AMS*

[31] WYLIE, D. P. and B. B. HINTON (1981) The feasibility of estimating large-scale surface wind fields for the summer MONEX using cloud motion and ship data, *Boundary Layer Meteorology*, 21, 357-367

[32] WYLIE, D. P. and B. B. HINTON (1982) A comparison of cloud motion and ship wind observations over the Indian Ocean for the year of the FGGE, *Boundary Layer Meteorology*, 23, 197-208